PACIFIC EARTHQUAKE ENGINEERING
RESEARCH CENTER

Seismic Performance of Isolated Bridges Under Beyond Design Basis Shaking

Claudio Sepulveda
Ricardo Bustamante
Gilberto Mosqueda

Department of Structural Engineering
University of California San Diego, La Jolla, California

PEER Report No. 2024/02

Pacific Earthquake Engineering Research Center
Headquarters at the University of California, Berkeley
February 2024

PEER 2024/02
February 2024

Seismic Performance of Isolated Bridges Under Beyond Design Basis Shaking

Claudio Sepulveda

Ricardo Bustamante

Gilberto Mosqueda

Department Structural Engineering
University of California San Diego, La Jolla, California

PEER Report 2024/02 Pacific Earthquake Engineering Research Center Headquarters at the University of California, Berkeley

February 2024

ABSTRACT

Seismically isolated highway bridges are expected to provide limited service under a safety evaluation-level ground shaking with minimal to moderate damage. The behavior under shaking beyond design considerations, corresponding to a large return period seismic hazard, is not well understood and could induce significant damage. In these rare events, the seismic isolation system can be subjected to displacement demands beyond its design capacity, resulting in failure of the bearings, exceeding the clearance and pounding against the abutment backwalls, or damage propagating to other primary structural components. To better understand the seismic performance of simple highway bridges subjected to earthquakes beyond design considerations, this study simulates the response of a prototype bridge structure and examines the lateral displacement demands, the transfer of forces to the substructure, and potential failure modes of seismically isolated bridges. Advanced modeling approaches are considered to capture bearing characteristics, such as hardening at large strains, and a pounding macro-element to capture the effects of impact. Results show that for beyond design shaking, the bearings can reach the maximum shear strain capacity, significant residual deformation of the abutment can result from pounding, and the columns can experience moderate damage. The progression of damage is identified in an effort toward the development of models suitable for assessing the overall seismic risk, repairability, and downtime of seismically isolated bridges.

Keywords: Bridge, Seismic Isolation, Beyond-Design Shaking, Pounding, Elastomeric Bearings

ACKNOWLEDGMENTS AND DISCLAIMER

This research study was funded by PEER, under Contract No. PBE – M7. The opinions, findings, conclusions, and recommendations expressed in this publication are those of the author(s) and do not necessarily reflect the view of Pacific Earthquake Engineering Research (PEER) Center, and the Regents of the University of California.

CONTENTS

LIST OF TABLES

LIST OF FIGURES

1 INTRODUCTION

Seismically isolated highway bridges are expected to provide limited service with minimal to moderate damage under safety evaluation level ground shaking, corresponding to a 1000-year return period. The behavior under extreme earthquakes, corresponding to larger return period seismic hazard, is less understood and could result in major damage leading to loss of service. In these rare events, the seismic isolation system can be subjected to displacement demands beyond its design capacity resulting in failure of the bearings, yielding of the columns, or exceeding the clearance and pounding against the abutment backwalls. Damage to the backwall is considered sacrificial as it can be repaired, and service restored within days (Caltrans 2019a). Nevertheless, pounding against the backwall can result in a large transfer of forces to the bridge deck, bearings, and piles and potentially amplify bearing displacements (Ruangrassamee and Kawashima 2001). Modes able to capture the progress of failure in seismically isolated bridges will lead to improved understanding of expected behavior and approaches for quantifying the risk of bridges under beyond-design basis shaking.

The National Bridge Inventory (NBI) database maintained by the Federal Highway Administration (FHWA 2020) lists 25,763 bridges in California, with about 1% being seismically isolated. Typically, seismic isolation has been considered when enhanced seismic performance is required, such as in critical routes of the highway systems relying on a continued operation (e.g., Caltrans bridges in Important and Recovery Bridge categories). Thus, seismically isolated bridges are often part of critical lifelines for which the seismic risk should be well understood. Further increasing the application of seismic isolation to include ordinary bridges can be an effective means to reduce damage and improve the reliability of the highway network.

The basic principle of seismic isolation applied to bridges is to uncouple the superstructure from the substructure. The uncoupling is achieved by placing low stiffness bearing devices at the deck interface, absorbing most of the deformation and limiting the transfer of inertial forces. The bearings are designed to deform laterally, providing energy dissipation and recentering capabilities. The low stiffness of the bearing elongates the fundamental period of vibration, which reduces the seismic demands in both the superstructure and substructure. The energy dissipation mechanism can be inherent in the bearing, such as friction, or added as supplemental devices to limit the lateral displacement and further reduces the seismic forces on the bridge substructures.

The application of seismic isolation for bridges can be most beneficial for cases where: (1) the bridge has stiff piers with a high natural frequency of vibration, (2) the bridge is nonregular, and (3) the expected ground motion is well-defined with a dominant high-frequency content, typical of shallow earthquakes, near-fault or rock sites (Priestley et al. 1996). There is little data to fully evaluate the performance of isolated bridges in earthquakes under strong ground shaking. In the U.S., the Sierra Point Overhead near the US 101 in San Francisco, CA, was the first bridge to be isolated. The bridge was constructed in the 1950s and retrofitted with seismic isolation in 1985.

During the 1989 Loma Prieta earthquake, no damage nor visible signs of distress (cracking or residual displacement) were observed (Kasai and Maison 1997). There are no reports of seismically isolated bridges subjected to shaking in Los Angeles during the 1994 Northridge Earthquake. In these past earthquakes in the U.S., however, there was reported damage to conventional bridges (Mitchell et al. 1991; Buckle et al. 1994). In Japan during the 1995 Kobe Earthquake, six isolated bridges suffered no damage while conventional bridges nearby had major structural damage (Robinson 1998). The 2008 Wenchuan Earthquake in China caused a permanent offset of elastomeric bearings and shear key failure, resulting in bridge span collapse (Li et al. 2008; Han et al. 2009; Xiang and Li 2018). Jonsson et al. (2010) report that the 2008 Earthquake that struck South Iceland damaged a 370m long base-isolated bridge with severe damage at the concrete blocks on all the piers, damage at the wingwalls and damage at the bridge deck due to contact with the abutment in the longitudinal direction. Seismic offset was also observed in the 1999 Chi-Chi and 2010 Chile Earthquakes (Kawashima et al. 2011). In the 2011 and 2016 Japan Earthquakes, bearings ruptured in shear, causing the separation of the substructure and superstructure (Kawashima 2012; Nishi et al. 2019).

Minimum design requirements for seismically isolated brides are provided in the reference manual (FHWA 2020), and local State Guidelines can provide specific design requirements. Caltrans Seismic Design Criteria (SDC) (2019a) provides recommendations for the modeling and analysis of highway bridges in California subjected to earthquake ground motions. The SDC requires evaluating the capacity and ductility of critical bridge components and systems. Earthquake Resisting Elements (EREs) are considered within the earthquake-resisting system to dissipate energy or increase the damping of the bridge during the design seismic hazards. Seismic isolation bearings are labeled as nonstandard EREs and are subjected to additional guidelines provided for designers (Caltrans 2019b). Caltrans (2019a) defines two categories for the bridge post-earthquake performance: damage state and service level. A seismically isolated bridge is labeled as 'Important,' for which the expected post-earthquake damage state under the Safety Evaluation Earthquake (SEE) is minimal to moderate. The response should be limited to essentially elastic behavior with limited repairs that would not require the replacement of the bridge and restoring operation within reasonable durations.

California bridges are designed for a seismic hazard with a 1000-year return period (Caltrans 2019a). In contrast, building design standards such as ASCE7-16 (2017) consider a seismic hazard level of a 500-year return period for design and a 2475-year return period for collapse prevention under the Maximum Considered Earthquake (MCE). While regular buildings may not require evaluations at the MCE, isolated buildings and the isolation system are designed for the MCE hazard level. The performance of seismically isolated bridges under beyond-design basis shaking is not currently examined as part of the design process. In addition, the seismic hazard field is constantly evolving, which could lead to an increase in the seismic hazard level for a given site and subject bridges to larger seismic demand than those imposed by earlier standards.

1.1 SCOPE AND OBJECTIVES

This report examines the seismic performance of a prototype highway bridge subjected to beyond-design basis shaking. The performance evaluation requires advanced modeling approaches to capture the progress of damage and potential failure modes. Thus, a significant effort of this research is towards developing models to capture the limit states of seismically isolated bridges. State-of-the-art models are employed to account for pounding between deck-to-abutments and bearing models considering limit states that include strength degradation and/or material hardening at large strains. These behaviors are important towards the estimation of the displacements in the isolation system and the transfer of forces to the substructure. Mitigation strategies are examined that have the potential to improve the performance of seismically isolated bridges under beyond-design basis shaking.

To develop state-of-the-art models of seismically isolated bridges, recent research is considered in applying seismic isolation to various types of structures. Lead rubber bearings (LRB) are applied for seismic isolation with behavior such as lead core heating and rubber hardening at large strains considered in recently proposed models (Marquez 2021). Detailed abutment models are also included to capture the effects of pounding. Observation from experiments shows a rebound effect following the first impact can result in increased displacements at reversals in subsequent excursion (Ruangrassamee and Kawashima 2001), amplifying demands on isolators and subsequent impacts. The properties of the contact material can thus be critical to the outcome of the response. Experimental and numerical studies, as well as detailed finite element models, are considered to verify the modeling approaches

2 LITERATURE REVIEW

2.1 SEISMIC HAZARD CHARACTERIZATION

Design codes define guidelines for the characterization of the seismic hazard for a given region. The seismic hazard intensity is correlated with the structure category and the expected post-earthquake performance. For bridges, Caltrans SDC (2019a) defines two seismic hazard evaluation levels: the Functional Evaluation Earthquake (FEE) and the Safety Evaluation Earthquake (SEE). The FEE represents an earthquake that has a significant chance of occurring during the lifespan of a bridge with a 20% probability of exceedance in 50 years (or a 225-year return period). The SEE represents a rare ground motion that may occur during the life of the structure. The SEE is given by a response spectrum based on a 5% probability of exceedance in 50 years (or a 975-year return period). This design spectrum is equivalent to having a 7% probability of exceedance in the 75 years of bridge life. Caltrans SDC (2019a) acknowledges that larger ground motions are possible without requiring additional design provisions. Lee Marsh and Stringer (2013) also recognizes the potential for larger ground motions in bridges especially in light of the risk-adjusted spectral accelerations for the 1,000-year design earthquake following recent changes in building design codes.

To define beyond design basis shaking, this study considers a rare earthquake with a 3% probability of exceedance in 75 years life of a bridge or a 2475-year return period. This is similar to the MCE hazard level considered for the design of building with base isolation (ASCE7-16 2017). It is recognized that Caltrans SDC (2019a) uses 975-year return period for the Safety Evaluation Earthquake (SEE), defined as a rare ground motion that may occur during the life of the structure. A larger return period is considered here to examine the behavior of bridges and the development of models considering that larger earthquakes may occur (Baker et al. 2011).

2.2 BRIDGE MODELS

The behavior of bridges under seismic loads has been widely studied (Buckle et al. 2006; Aviram et al. 2008; Konstantinidis et al. 2008; Kaviani et al. 2012; Kaviani and Zareian 2014; Tsiavos et al. 2014; Deb et al. 2018). Aviram et al. (2008) provide an extensive literature review of engineering practice and code criteria for bridge design, modeling, and analysis. Modeling guidelines for the material and mass properties of primary components, including the superstructure, cap beam, abutment, and pier are provided. Depending on the bridge category and the analysis type, models varying from simplified models to detailed nonlinear models can be developed. Caltrans (2019b) specifies the minimum requirements to perform a Nonlinear Time History Analysis (NTHA), with a model considering the soil-foundation-structure interaction, gaps, and impact on gap closure, multiple support excitations, isolation damper devices, and

nonlinear soil, material, and hysteretic behavior. State-of-the-art models consider linear elastic beam elements for the bridge deck and nonlinear beam-column elements for the columns or piers. The soil-foundation system can be modeled with linear and rotational springs. The longitudinal and transverse stiffnesses of the abutment are incorporated using bilinear models. As an example, Deb et al. (2021) developed a state-of-the-art three-dimensional nonlinear analysis bridge model based on nonlinear fiber-section beam-column elements and nonlinear springs. A similar detailed model was developed by Rezaei et al (2020) to study the effects of pounding and irregularity on the seismic behavior of typical concrete box-girder bridges with unequal-height piers.

2.3 DAMAGE LIMIT STATES

Zhang and Huo (2009) summarized the definitions of various damage states and damage index criteria available in the literature for seismically isolated bridges to study the effectiveness and optimum design parameters for isolation devices. The damage states for elastomeric isolation devices were defined based on bearing shear strain, considering 250% shear strain as complete damage, although bearings can sustain up to 400% shear strain (Masroor et al. 2013). However, at 250% shear strain, the isolation system will experience a large displacement that could cause pounding or unseating. Ramanathan (2012) proposed Component Damage Thresholds (CDT) for Primary and Secondary Elements, grouping damage state definitions according to similar consequences related to repair and traffic implications following a seismic event. The data they derived aligns with the Caltrans Design Code (2019b). They characterized the bridge elements in two types, based on whether the vertical stability is affected or not. The CDT values, organized in four levels, can be described using a prescriptive or descriptive approach, or both (Padgett et al. 2008) if using Bayesian updating principles. Notably, for the prescriptive approach based on the mechanics, a functional level is associated with component damage such as spalling of the cover concrete in a column, buckling or rupture of the longitudinal column reinforcement, etc.

The Caltrans Seismic Design Code (2019b) assesses the seismic performance of bridges based on the Post-Earthquake Damage Level of Seismic Critical Members (SCMs). Three damage states after Vosooghi and Saiidi (2010) are considered: major damage associated with imminent failure; moderate damage related to extensive cracks and spalling and visible lateral or longitudinal reinforcing bars; minimal damage associated with flexural cracks, and minor spalling and possible shear cracks. The Design Philosophy of Caltrans follows the "strong beam - weak column" principle with capacity design, where specific elements are designed for energy dissipation. When seismic isolation is used, the design approach is such that the bearings are meant to be the energy dissipation source. The addition of bearings is intended to reduce seismic design forces by increasing the period of a relatively stiff bridge, limiting the inertial forces transferred between the superstructure and substructure. Potential plastic hinging elements may still occur; columns must satisfy the same ductility requirements, ranging from 2.5 to 5.0.

2.4 BEARING MODELS

Lead-rubber bearing bearings (LRB) are considered for the protype bridge in this study, though the results can be applicable to other types of bearings. LRB are composed of layered elastomeric pads and steel shims with a lead plug insert for energy dissipation. The behavior of LRB through the expected range of design level loading is typically represented by a bilinear model, as shown in Figure 2.1. LRB exhibits more complex behavior when subjected to large amplitude cyclic displacement, including strength degradation due to heating of the lead core, P-Δ effects, strain hardening of the rubber and lead, as well as vertical-horizontal coupling with the axial load. While dependent on the material used, rubber hardening can initiate around 250% shear strain in the rubber and can achieve over 400% shear strain prior to bearing failure (Marquez 2021).

Several LRB models have been developed based on observed responses under cyclic loading (Kumar et al. 2015; Kikuchi and Aiken 1997). More recently, Marquez (2021) proposed a mathematical model using data from large bearings tested through failure. The proposed Large Strain Lead Rubber Bearing (LSLRB) model considers three nonlinear springs acting in parallel: a hysteretic model, a hyperelastic model, and an unloading model. The hysteretic model accounts for the heating of the lead and the initial lead hardening, the hyperelastic model accounts for the hardening effects at large strains and damage parameters, and the unloading (hysteretic) model accounts for the unloading effects that are seen at higher strains, as shown in Figure 2.2. Figure 2.3 compares the typical bilinear model, the LeadRubberX model, (Kumar et al. 2013), which captures strength degradation due to lead core heating, and the LSLRB model. The three models were first calibrated to the same experimental data set, then earthquake simulations were conducted for a single-degree-of-freedom (SDOF) system to examine the variation in responses under earthquake loading. The LSLRB estimates a lower lateral displacement for this simulation to large strains that engage hardening behavior in the rubber.

2.5 CONTACT MODELS

Seismic pounding can be modeled using contact elements consisting of uniaxial springs and a dashpot placed at the interface of two colliding bodies. The localized deformation at the contact is referred to as indentation and can be expressed in terms of relative displacement. The contact element considers a gap for activation, which is defined as the physical distance at rest between the two bodies. The impact has two phases that should be considered for modeling; the approach and the restitution. The maximum force does not necessarily happen at the maximum indentation. Several models have been proposed, from linear elastic springs to nonlinear contact model types. For example, a contact model, such as the Hertzdamp model, relates the impact force to the indentation using a power law, adding a quasi-viscous component to represent the velocity-dependent part. Many existing models (Lankarani and Nikravesh 1990; Muthukumar and DesRoches 2006; Jankowski 2005) depend on the indentation rate, which can be difficult to define. These models typically require calibration and rely on experimental data of material indentation.

Hughes (2020) improved upon existing contact element models available in structural analysis simulation software. A contact model was implemented in OpenSees (McKenna et al. 2010) and was developed based on experimental data and detailed finite element analysis of base isolated buildings considering nonlinearity in the superstructure and moat wall behavior (Sarebanha et al. 2018). The contact model is based on the Hertzian law of contact. Fundamental system property parameters are required, such as the Poisson ratio (ν), Young's modulus (E), body volume (V), and body mass (m). Each colliding body provides one set of parameters and simplifies the expressions here using notation of subscript 1 for the moat or retaining wall and subscript 2 for the superstructure. The hertz stiffness (kh) is defined as:

$$k_h = \frac{4}{3\left[\left(\frac{1-\nu_1^{\,2}}{E_1}\right)+\left(\frac{1-\nu_2^{\,2}}{E_2}\right)\right]\sqrt{\left(\frac{4\pi}{V_1}\right)^{1/3}+\left(\frac{4\pi}{V_2}\right)^{1/3}}}$$

The force indentation relationship is:

$$f_c(t) = k_h \delta(t)^{3/2} + c_h \dot{\delta}(t)$$

where d(t) are the material indentation and t the material indentation velocity. The Hertz damping coefficient (ch) is defined as:

$$c_h(t) = \xi_h \frac{k_h}{\delta_0} \delta(t)^{3/2}$$

The damping coefficient (ch) depends on the pre-impact indentation velocity (v0), which is the velocity just before the colliding bodies come into contact, and the Hertz damping ratio (ξh), expressed as:

$$\xi_h = \frac{8}{5} \cdot \frac{1-e}{e}$$

were (e) is the coefficient of restitution.

2.6 CONTACT MODELS

Particularly for base isolated structures, structural pounding occurs between the superstructure and the surrounding wall or abutment. Pounding has been observed between base-isolated buildings and their retaining walls, between adjacent buildings, bridge segments, and bridge-abutment interfaces. Two colliding bodies with different strengths, stiffnesses, and masses interact over a very short duration at a relatively small surface, introducing high-frequency waves. Multiple nonlinearity sources, such as material, geometric, and contact nonlinearity, must be considered for modeling purposes. Several analytical studies have been conducted to study this phenomenon on base-isolated buildings, focusing on developing a contact element capable of capturing all these nonlinearities and studying the pounding effects on the superstructure. Fewer analytical and experimental studies have been conducted on structural pounding in base-isolated bridges.

DesRoches and Muthukumar (2002) showed that the characteristic period of ground motion and the frame stiffness ratio primarily affect the pounding responses in a multi-frame bridge. They

found that pounding reduces the frame response when vibrating near the characteristic period of the ground motion. The effect of restrainers on the pounding response was evaluated, showing that restrainers do not change the demand if pounding occurs. Kun et al. (2017) experimentally studied the effects of skew angle and pounding on a bridge–abutment system under seismic excitation, showing that pounding increases the pier bending moment and relative lateral displacements.

Rezaei et al. (2020) assessed the effects of pounding on the seismic behavior of typical concrete box-girder bridges. Two pounding zones were studied: the seat-type abutment and the in-span hinge of multi-frame bridges. The focus of this study was to quantify the effects of pounding on the Engineering Demand Parameters (EDPs), including the Intensity Measure (IM) and different earthquake returning periods. They quantified the pounding force for regular and irregular pier configurations using the difference between the spectral displacement of the first longitudinal mode and the gap size as the metric. The study concluded that the gap clearance has the highest effects on the abutment, the pounding force, and the base shear, with a lesser effect on the unseating, the bearings, and the columns. On the clearance, Jankowski (2017) showed that pounding might have two patterns. For a small clearance, more pounding instances with lower peak pounding forces are expected, while for a large clearance, few collisions are expected with larger peak pounding forces, potentially leading to structural damage.

An experimental and numerical study by Jiao et al. (2021) shows that unevenly distributed pounding forces can significantly increase the relative radial displacement of the deck corners of a curved bridge. The experimental data shows that the pounding force peak value and the number of pounding instances decrease if the distance between expansion joints increases, that the structures are more likely to collide under near-fault ground motions, and that the location of pounding mostly occurs at the corner of main beam, and the number of pounding instances inside the curve is larger.

A structural pounding study on an existing multi-span curved girder bridge in South California was done by Malhotra et al (1995) using the California Strong Motion Instrumentation Program (CSMIP). The study concluded that the acceleration pulse generated by the pounding propagates along the bridge. While the peak ground acceleration at the bridge site was only about 0.10g for the two earthquakes recorded, the highest spikes recorded on the bridge were 0.80g and 1.0g. The spikes were caused by forces generated at separation joints by impacts and stretching of the cable restrainers between adjacent bridge segments.

For design, Caltrans (2019b) does not address pounding or mitigation strategies. Past studies indicate the most critical EDPs related to the pounding are the clearance and the impact velocity. Mitigation strategies to reduce the pounding effects should explore increasing the clearance, if feasible, or reducing the impact velocity.

Mitigation strategies that could influence both the clearance and the impact velocity while minimizing the increase in base shear for design-level shaking include supplemental damping or engaging stiffening in the seismic isolation system. For example, LRB exhibit strain hardening that can be initiated once the design displacement is exceeded. Similarly, friction sliding bearings

have been designed to have stiffening regime at large displacements (Fenz and Constantinou 2008). The bearing design could be tailored to engage stiffening before pounding, reducing the impact velocity and the lateral displacement. In LRB, for example, strain hardening can be achieved by varying the number and thickness of rubber layers while maintaining similar effective properties. Design guidelines do not specify an allowable shear strain but specify strain hardening can occur after 150% of the design displacement demand of the isolation bearing (DT).

The abutment backwall is designed for soil lateral pressure, and it is not detailed to account for pounding forces. Pounding of the deck against the backwall can damage the joints between the abutment and the backwall, imposing considerable pressure on the backfill and severely damaging the backwall potentially disrupting traffic. The backwall failure mode and strength contribution due to pounding are unknown, hence a comprehensive finite element model is first examined to estimate the backwall capacity and to assess the damage state.

CHAPTER 2: FIGURES

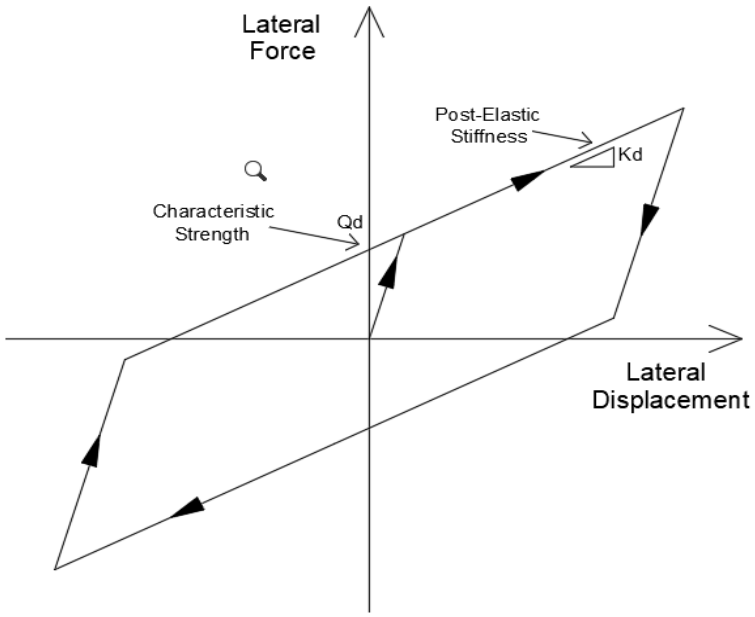

Figure 2.1 Idealized lateral force-lateral displacement loop for a lead-rubber bearing

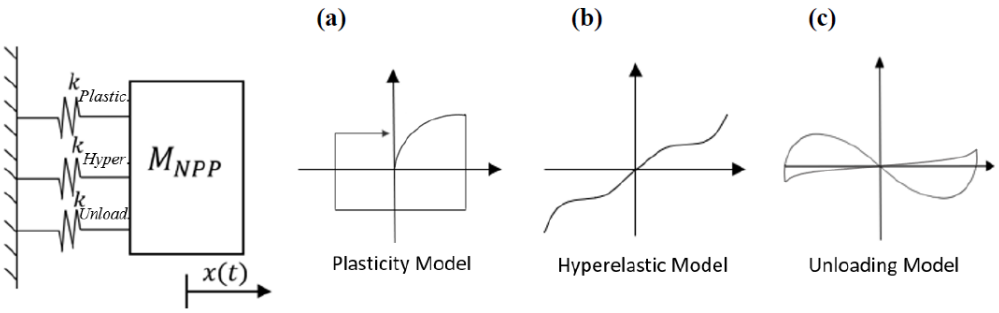

Figure 2.2 Parallel System. (a) Plasticity (heating and LH) model, (b) Hyperelastic (rubber hardening) model, (c) Unloading (Hysteretic) model

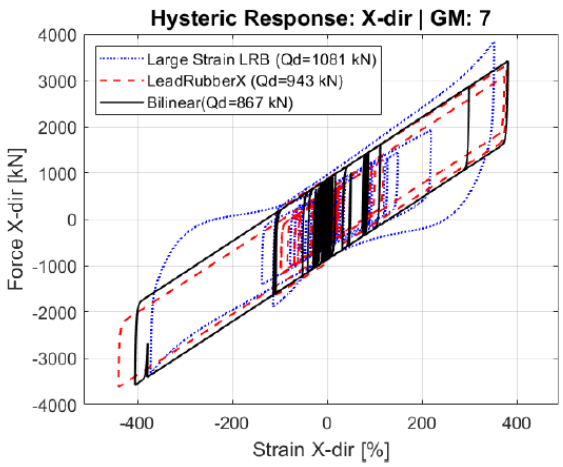

Figure 2.3 Bearing models responses subjected to a single ground motion

3 PROTOTYPE BRIDGE MODEL

3.1 BRIDGE MODEL

A model of a prototype bridge is developed for nonlinear analysis in OpenSees. The bridge is based on a design example by Constantinou et al. (2011) that is a modification of an ordinary bridge presented in Buckle et al. (2011). The bridge is 320 feet long with three-spans at 100-120-100 feet and a cast-in-place concrete box girder deck, as shown in Figure 3.1. Each bent is composed of two circular columns 20 feet tall, 4 feet in diameter, and a cap beam supporting the bearings. The original design includes a skew angle of 30º which was removed as part of the modification for isolation design. The assumed clearance between the deck and abutment backwall equals 21 inches. No shear keys were considered in the transverse direction; therefore, there are only restraints and potential for pounding in the longitudinal direction.

The bridge model assumes a rectangular cross-section for the deck designed to remain elastic for service and seismic loads. The entire deck is divided into several elastic beam-column elements, with the mass lumped at the translational and rotational DOFs. The column bases are rigidly connected to the footing that is supported on a set of six DOF linear elastic springs to simulate the flexibility of the foundation. The model elevation is shown in Figure 3.2.

Figure 3.3 shows the analysis model for the bent, using elastic beam-column elements with a gross section according to the original design. For the columns, distributed plasticity displacement-based elements are used. To minimize localization problems at the element level due to the softening behavior of concrete, one element is used for each of the two ends and another element for the middle zone of the columns (Coleman and Spacone 2001; Scott and Fenves 2006). The length of each element at the column ends was computed such that it is equal to the expected plastic hinge length according to the empirical expression proposed by Paulay & Priestley (1992). For material properties, nominal values are used according to the design for the strength of steel and unconfined concrete. For confined concrete, the compressive strength was computed using the expression proposed by Saatcioglu and Razvi1 (1992), and the ultimate strain using the expression by Scott (1980). The material model used for concrete is Concrete02 and for reinforcement steel is SteelMPF. Table 3.1 summarizes the material properties used for the columns.

Caltrans (2019b) requires that the material properties used in the NTHA are based on the expected material properties since they provide a more realistic estimate of the design strength (Unanwa and Mahan 2014), with an exception for the shear capacity, which is based on the specified material strengths. The analyses presented in this report use nominal properties for bearings, concrete, and steel materials. A Rayleigh damping ratio of 2% proportional to the initial stiffness was added, following the guidelines for isolated structures from Hall (2018) and Ryan & Polanco (2008). This approach avoids introducing excessive energy dissipation to the first modes due to the mass-

proportional damping components of the deck behaving as a rigid body. Stiffness proportional damping was not added to the bearing elements.

3.2 BRIDGE MODEL

Considering the response of isolated bridges beyond design considerations, bearing models able to capture behavior at large shear strains are considered. The large strain lead rubber bearing (LSLRB) model developed by Marquez (2021) is used since it considers the combined effects of lead core heating and material strain hardening in the lead and rubber. The selection of the model parameters for the size of bearings considered in this analysis is based on data available in the literature for similar size, and axial pressure (Nakamura 2012; Feng et al. 2004; Nishi et al. 2019; Domaneschi et al. 2018; Yamamoto et al. 2008). Experimental data from bearings tested up to a maximum shear strain of 400% was used to calibrate the model.

3.3 ABUTMENT-BACKFILL SOIL-POUNDING INTERACTION

Pounding can be expected for isolator displacements exceeding the clearance to the abutment. In this case, the deck pounds against the abutment backwall interacting with the backfill soil. To characterize this interaction, the abutment is separated into subsystems characterized individually and assembled into a macro-model for the analysis in OpenSees. Previous studies for the backfill soil characterization (Wilson and Elgamal 2010) and contact model (Hughes and Mosqueda 2020) are used. However, to better derive the model for the abutment, detailed finite element analysis model were examined to identify overall behavior, potential failure modes, and capacity of elements during impact.

Figure 3.4 shows the proposed macro-model, which was developed using discrete cantilevers composed of elastic beam-column elements with lateral and base shear springs to capture the nonlinear response of the backwall, nonlinear soil springs to capture the backfill, and a contact model to capture the deck pounding.

3.3.1 Abutment model

A finite element model was first developed in Abaqus[1] considering a standard seat-type abutment geometry and components, as shown in Figure 3.5. The Abaqus model uses a 3D deformable solid, linear geometry, reduced integration elements for the concrete, and 2-node linear 3D truss elements for the steel rebar. The concrete material is modeled using a Concrete Damaged Plasticity model with nominal strength of 24.5 MPa, Young's modulus of 26,743 MPa, and Poisson's ratio equal to 0.20 with additional properties listed in Table 3.2. The stress-strain relationship is modeled after Chang and Mander (1994). The material model properties in compression are shown in Figure 3.6, while the properties in tension are shown in Figure 3.7. The steel material is modeled using a

[1] ABAQUS (2020), Dassault Systemes Simulia, Inc.

plastic model with isotropic hardening with yield strength of 413.7 MPa, Young's modulus of 200,000 MPa, and Poisson's ratio of 0.30. The ultimate tensile strength is considered as 620.5 MPa at a strain of 0.20.

The Abaqus abutment model is shown in Figure 3.8. Using static analysis, the lateral deck footprint is used to apply an incremental displacement on the backwall. Gravity loads and concentrated loads for the bridge weight are also applied. The damage pattern of the concrete in tension is shown in Figure 3.9 with nonlinear behavior concentrated at both sides of the backwall due to the change in stiffness between the bulk concrete sections and the slender backwall section. Two shear zones can be observed, one for the lateral shear force and one for the base shear force. Figure 3.10 shows the lateral shear force versus lateral (out-of-plane) displacement of one of the backwall sides, while Figure 3.11 shows the base shear force. The results show a limited contribution of the backwall when compared to the bridge weight. It is assumed that the backwall has no ductility with a rapidly degrading strength once the rebar yields. These results suggest that the backwall can be characterized by nonlinear shear springs located at the base and sides of a rigid element.

3.3.2 Abutment model

A simplified macromodel of the abutment was developed for nonlinear time history analysis in OpenSees. The model aims to capture the behavior observed in the finite element model presented in the previous section. The Hertzdamp model (Lankarani and Nikravesh 1990) was used to represent the impact interface between the abutment and the bridge deck. This contact model has been verified based on experimental data of seismically isolated buildings pounding against a moat wall (Masroor and Mosqueda 2013). This model was implemented in OpenSees as a material class, then used within a truss element to connect the two substructures. The uniaxial Hertz contact element is placed at the impact location (Hughes 2020), assuming a coefficient of restitution equal to 0.7. The Hertz nonlinear stiffness (kh) is obtained by assuming a colliding sphere of radius equal to the 800mm isolation slab depth to a massive plane surface, obtaining a value of kh=14955141 kN/m.

Nonlinear soil springs at the top of the wall and impact location represent the backfill soil (Sarebanha 2018). The springs are defined by an HyperbolicGapMaterial model at two levels with properties equivalent to a T2 soil based on Wilson and Elgamal (2010): at one-meter height, equivalent to the backwall mid-height, and at two meters height, equivalent to the top of the backwall. The unloading/reloading stiffness is defined equal to the initial stiffness, with a failure ratio equal to 0.7 and no initial gap.

3.4 RESPONSE SPECTRUM AND GROUND MOTION SETS

Nonlinear time-history analysis is performed on the bridge model using 30 bidirectional ground motions obtained from the NGA-West2 database (Ancheta et al. 2012). The seismic hazard is associated with a return period of 2475 years for a bridge located in California on soil with a shear wave velocity (Vs30) equal to 360 m/sec. A Uniform Hazard Response Spectrum (UHS) is

obtained from the Unified Hazard Tool (USGS 2022) as shown in Figure 3.12. The ground motions are scaled following the Conditional Spectrum method (Baker et al. 2011; Baker and Lee 2018), using the tool developed by Baker (2011). The conditioning period is defined as 2.5 sec, and the maximum scaling factor is equal to 4. The response spectra for the scaled ground motions are shown in Figure 3.13, and all the ground motion statistics are shown in Table 3.3. For the Safety Evaluation intensity ground motions, the above-mentioned set of records was downscaled by a constant factor equal to the ratio between the UHS ordinate of 2475 years and 975 years of return period at the target period, which is 1.4. This approach was preferred instead of choosing another set of records and to use the same ground motions for comparison between intensities.

CHAPTER 3: TABLES

Table 3.1 Material properties for concrete

Type	f'c (MPa)	ec0	fcu (MPa)	ecu
Cover	27.58	0.00200	1.38	0.00400
Core	36.65	0.00266	14.66	0.01525

Table 3.2 Concrete Damaged Plasticity parameters

Dilation Angle	Eccentricity	fb0/fc0	K	Viscosity Paramater
38	0.10	1.16	0.666	0

Table 3.3 Ground motion sets scale factors

Record Number	Record Sequence Number	Earthquake Name	Station Name	Magnitude	Year	Scale Factor
1	5810	Iwate, Japan	Machimukai Town	6.9	2008	2.46
2	884	Landers	Palm Springs Airport	7.28	1992	3.87
3	2457	Chi-Chi, Taiwan-03	CHY024	6.2	1999	2.51
4	5827	El Mayor – Cucapah, Mexico	Michoacan de Ocampo	7.2	2010	1.4
5	6912	Darfield, New Zealand	Hulverstone Drive Pumping Station	7	2010	2.63
6	6952	Darfield, New Zealand	Papanui High School	7	2010	1.4
7	4875	Chuetsu-oki, Japan	Kariwa	6.8	2007	0.42
8	1534	Chi-Chi, Taiwan	TCU107	7.62	1999	1.66
9	292	Irpinia, Italy-01	Sturno (STN)	6.9	1980	1.69

Record Number	Record Sequence Number	Earthquake Name	Station Name	Magnitude	Year	Scale Factor
10	2509	Chi-Chi, Taiwan-03	CHY104	6.2	1999	2.71
11	1539	Chi-Chi, Taiwan	TCU113	7.62	1999	3.37
12	3270	Chi-Chi, Taiwan-06	CHY030	6.3	1999	3.15
13	8130	Christchurch, New Zealand	Shirley Library	6.2	2011	1.41
14	1536	Chi-Chi, Taiwan	TCU110	7.62	1999	1.14
15	1547	Chi-Chi, Taiwan	TCU123	7.62	1999	2
16	2114	Denali, Alaska	TAPS Pump Station #10	7.9	2002	1.14
17	1045	Northridge-01	Newhall - W Pico Canyon Rd.	6.69	1994	1.22
18	1063	Northridge-01	Rinaldi Receiving Sta	6.69	1994	1.48
19	1535	Chi-Chi, Taiwan	TCU109	7.62	1999	1.55
20	1492	Chi-Chi, Taiwan	TCU052	7.62	1999	0.77
21	569	San Salvador	National Geografical Inst	5.8	1986	3.07
22	171	Imperial Valley-06	El Centro - Meloland Geot. Array	6.53	1979	1.3
23	5786	Iwate, Japan	Minamikatamachi Tore City	6.9	2008	2.21
24	1762	Hector Mine	Amboy	7.13	1999	3.95
25	4847	Chuetsu-oki, Japan	Joetsu Kakizakiku Kakizaki	6.8	2007	2.22
26	527	N. Palm Springs	Morongo Valley Fire Station	6.06	1986	2.69
27	786	Loma Prieta	Palo Alto - 1900 Embarc.	6.93	1989	2.77
28	3746	Cape Mendocino	Centerville Beach_ Naval Fac	7.01	1992	2.6

Record Number	Record Sequence Number	Earthquake Name	Station Name	Magnitude	Year	Scale Factor
29	159	Imperial Valley-06	Agrarias	6.53	1979	3.32
30	1238	Chi-Chi, Taiwan	CHY092	7.62	1999	2.87

CHAPTER 3: FIGURES

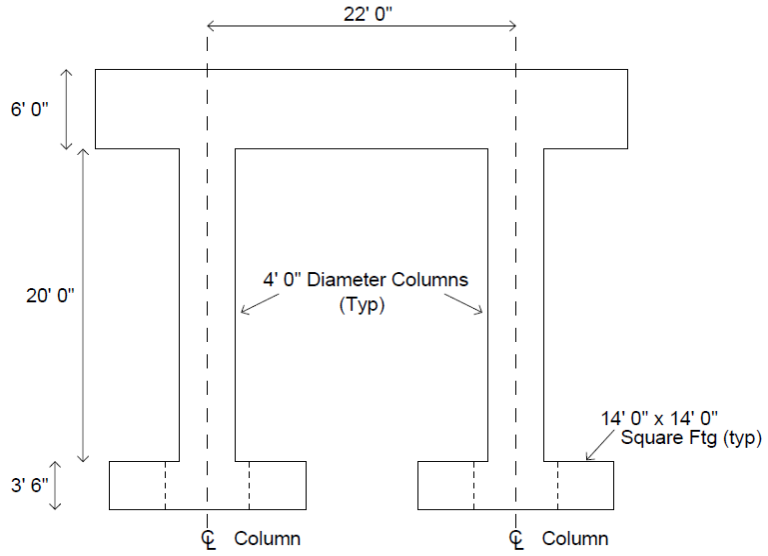

Figure 3.1 Bridge bent elevation

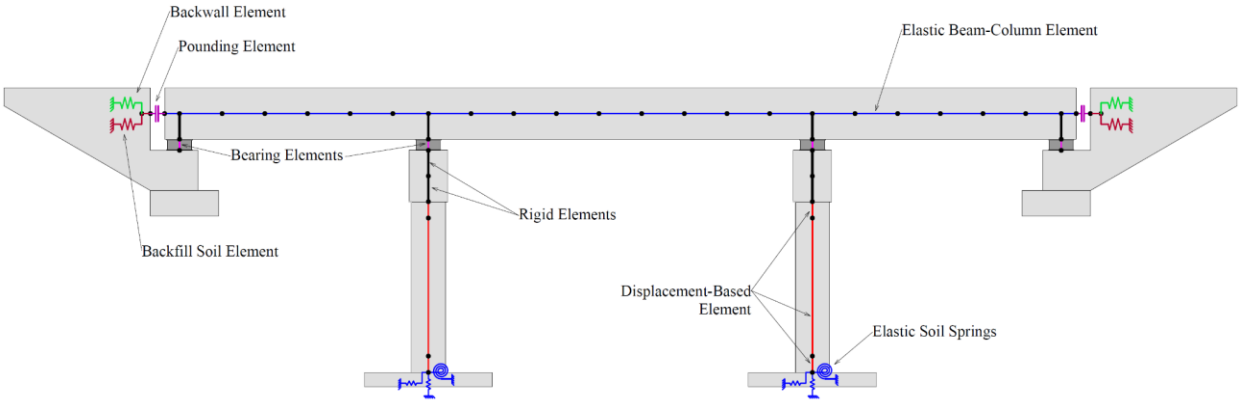

Figure 3.2 Elevation of bridge and element modeling scheme

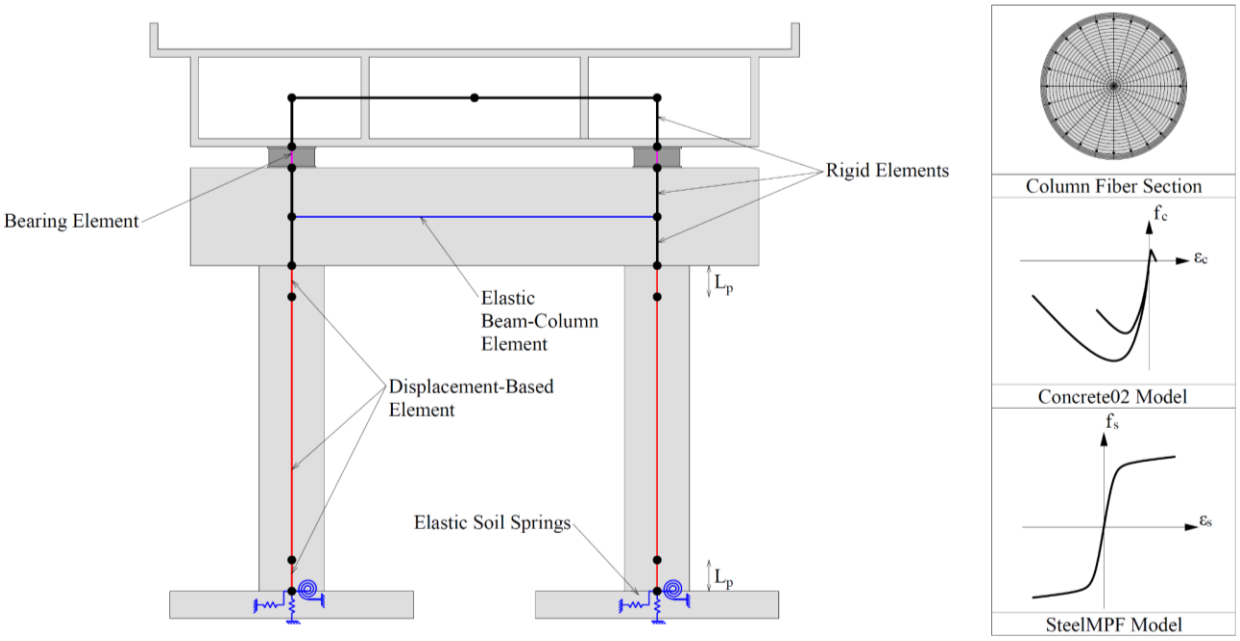

Figure 3.3 Bent modeling element scheme

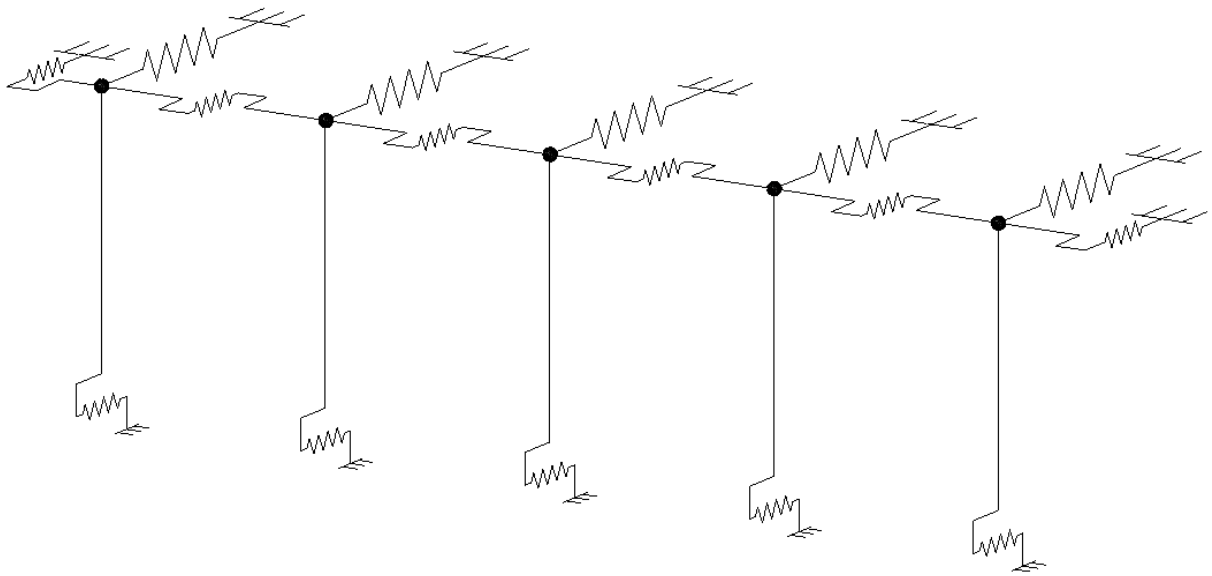

Figure 3.4 Simplified abutment model in OpenSees

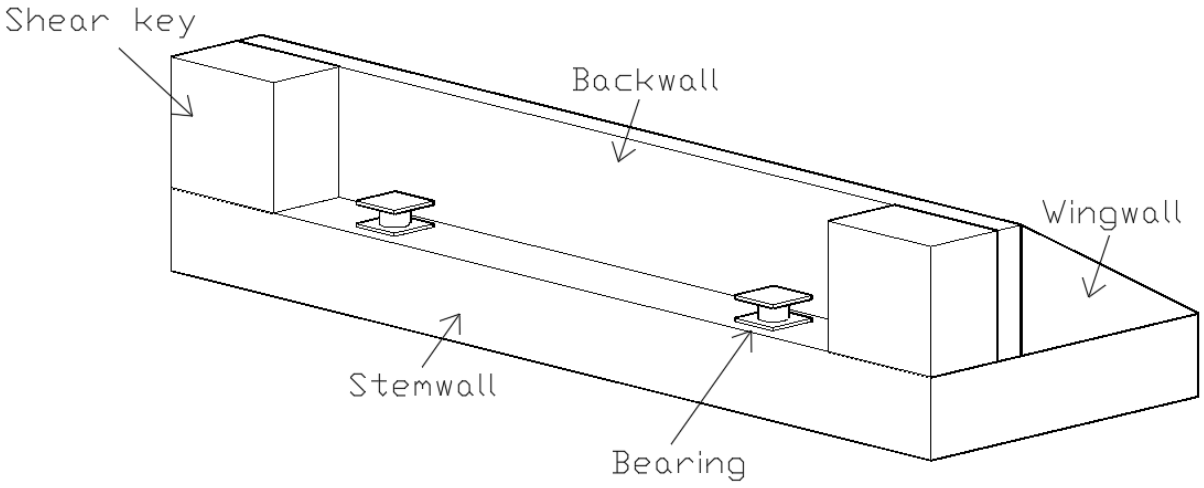

Figure 3.5 Abutment model overview

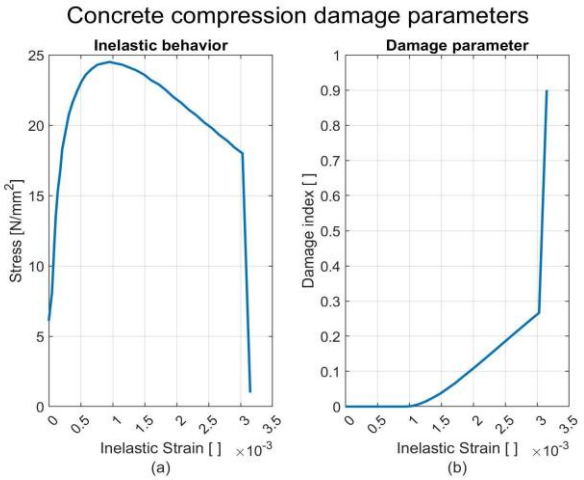

Figure 3.6 Concrete compression damage parameters

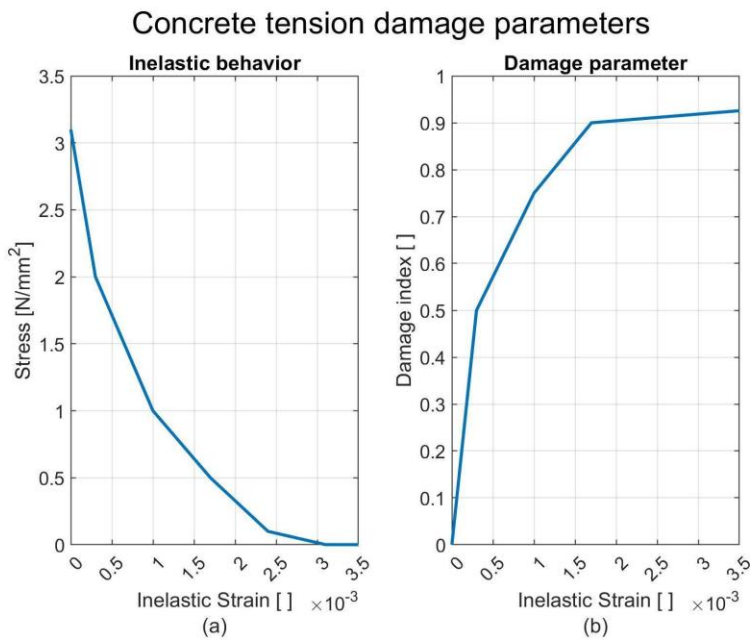

Figure 3.7 Concrete compression damage parameters

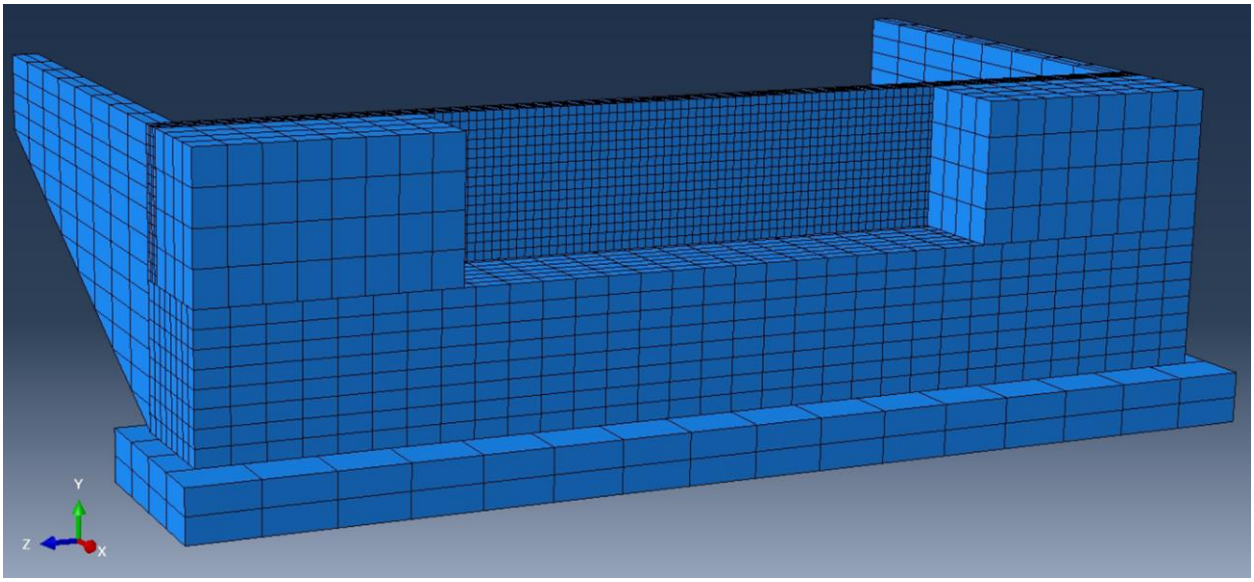

Figure 3.8 Abutment finite element model in Abaqus

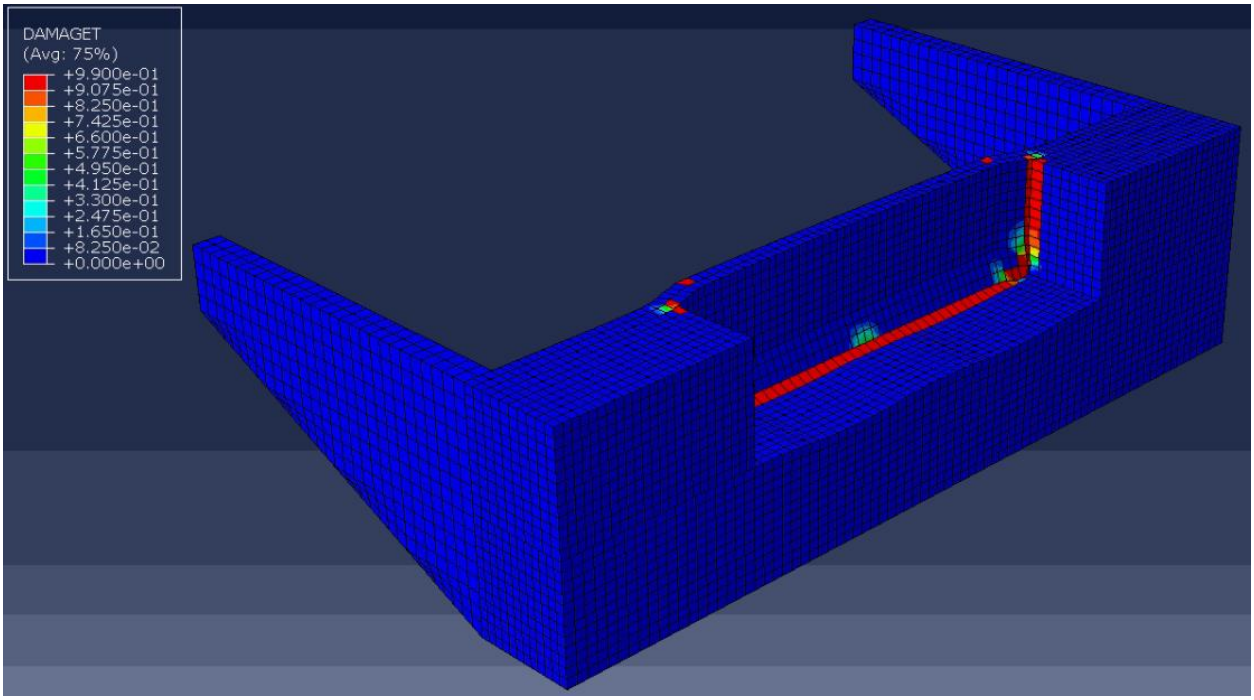

Figure 3.9 Damage pattern for lateral loads

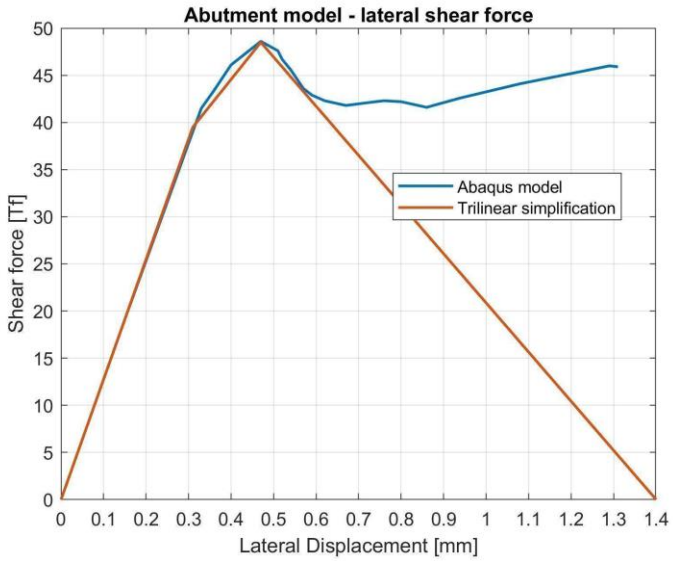

Figure 3.10 Lateral shear force versus lateral displacement

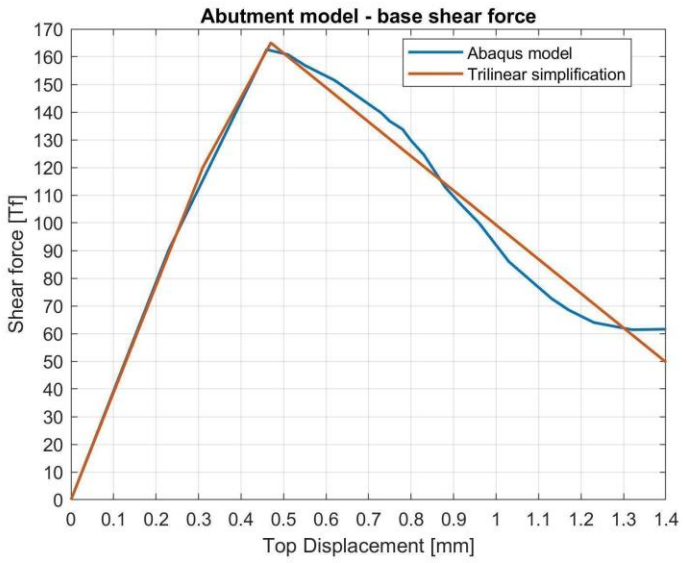

Figure 3.11 Base shear force versus lateral displacement load

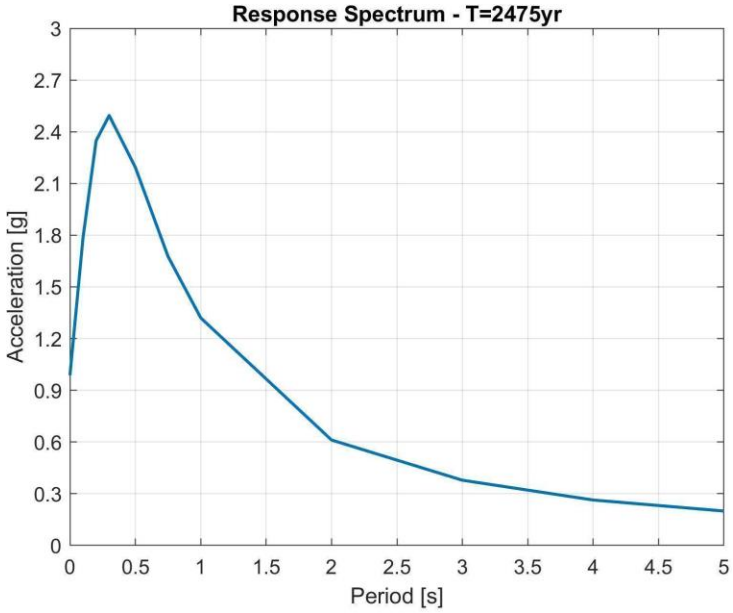

Figure 3.12 Uniform Hazard Response Spectrum for T=2475yr

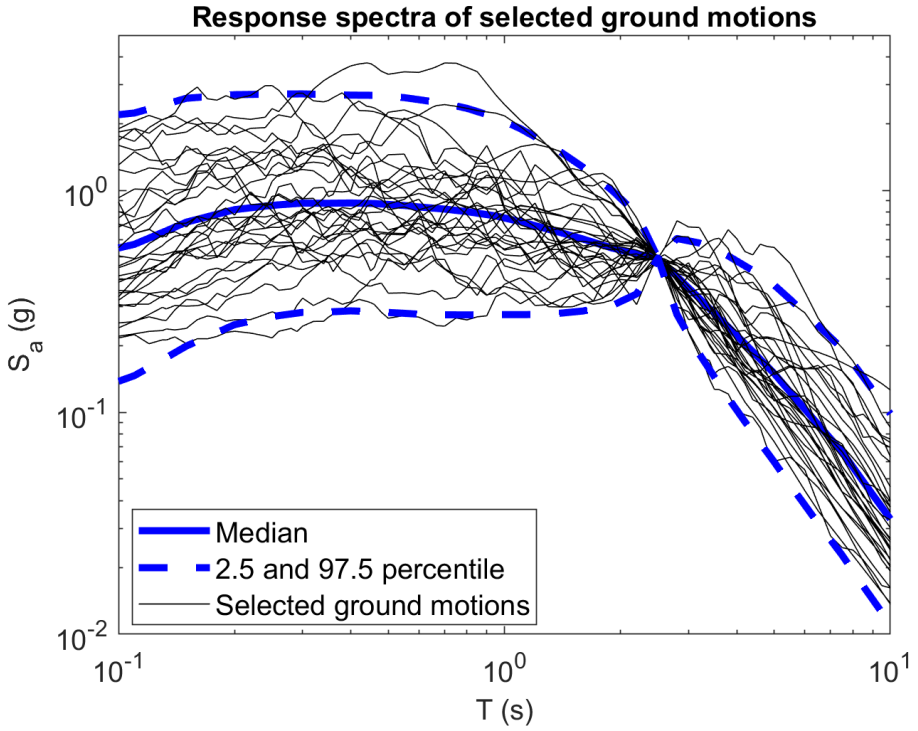

Figure 3.13 Uniform Hazard Response Spectrum for T=2475yr

4 SIMULATION RESULTS OF PROTOTYPE BRIDGE

The seismic response of the prototype bridge is evaluated for the set of 30 pairs of horizontal earthquake records scaled to two different hazard intensities. The detailed response of the bridge is first shown for one record at both intensities to gain insight on the level of nonlinear behavior and progress of damage. A summary of the maximum response parameters obtained for all records is then presented. Design alternatives to enhance the performance for beyond-design shaking are evaluated and compared to the original design.

4.1 DETAILED RESPONSE ANALYSIS FOR DESIGN AND BEYOND DESIGN SHAKING

The response of the bridge and its components is presented for the two sets of motion scaled to the design level intensity associated with a return period of 975 years, and the beyond-design level intensity associated with a return period of 2475 years. The detailed response of the bridge subjected to the Chuetsu-oki records scaled by 2.22 and labeled as ‘Record 25’ is presented first.

Figure 4.1 shows the orbital displacement of the deck relative to its supports. The dashed line represents the clearance of the abutment backwall; exceeding this limit indicates impact. There are no restraints in the transverse direction. No impact is observed for the design level intensity, while there is one impact at the west abutment for the record scaled to beyond-design level. The bridge response associated with the backwall pounding will be examined in more detail later. It is important to note that there was no significant deck rotation due to model symmetry in these simulations that could amplify bearing displacements.

The bearing hysteresis of one of the isolators at the west abutment is shown in Figure 4.2 for both intensity levels. The shear force is normalized by the weight of the deck, and the lateral deformation is normalized as the shear strain of the rubber (deformation/height of rubber). For the design level ground motion, the bearing exceeded 250% of the shear strain in the transverse direction, showing slight hardening in the response after 200% shear strain. The increased displacement demands for beyond-design level shaking result in significant hardening, reaching about 300% shear strain in the longitudinal direction and about 350% for the transverse direction. The hardening seems more excessive in these simulations compared to experimental data due to a bi-directional effect discussed later.

Of particular interest in this study is the distribution of demands between the isolators and bent with increasing earthquake intensity. This is because the effectiveness of seismic isolation can be reduced at the onset of yielding with deformation demands shifting to other structural components.

To examine the response of the bent, Figure 4.3 shows the demands on the plastic hinge for one of the columns at the west bent. Both bottom and top plastic hinge element responses are shown. The column remains mostly linear for the design level intensity as expected for a seismically isolated bridge. A significant difference in demand is shown between longitudinal and transverse directions, with a small deformation demand for the top hinge in the longitudinal direction likely due to the predominant cantilever deformation of the bent and the flexibility of the rubber bearing. The frame action in the transverse direction results in larger moments at the top of the columns. The deformation demands increase significantly for the beyond-design intensity, resulting in a nonlinear incursion in both directions with the largest demands in the longitudinal direction. From Figure 4.4 the overall bent response also shows an increase in inelastic incursion as observed for the west bent base shear versus drift ratio. Since column hinge response is cleaner and more representative of damage to the bent, the following sections focus on this component behavior to observe the bridge bent response.

4.1.1 Evaluation of Maximum Demands

The maximum response values for all the records considered are obtained from nonlinear time history analysis. All the ground motions were sorted in ascending order based on the maximum orbital deck displacement for the 2475yr return period of the original design. This order remains the same for subsequent analyses. Figure 4.5a) shows the maximum value of the deck displacement orbit. This value is computed as $\sqrt{{u_x}^2 + {u_y}^2}$, where u_x and u_y are the displacements of the deck for the longitudinal and transverse directions, respectively. It can be observed that the ratio between the maximum deck displacements for both intensities is on average about 2.0, while the scale factor between the input ground motions is about 1.4. The maximum deck displacement in each orthogonal direction is shown in Figure 4.5b), where the dashed line represents the gap clearance with the abutment. There is no impact for design-level intensity ground motions. In contrast, for the beyond design intensity, the maximum longitudinal displacement exceeds the abutment clearance in 11 out of 30 ground motions.

Figure 4.6 shows the maximum rotation in the column plastic hinge. For design level intensity, few ground motions exceed the yield level of 2e-3 radians associated with yielding and onset of nonlinear behavior, and only for the longitudinal direction. Then, for design level, there is only slight yielding and only in the weaker direction. On the other hand, for the beyond design intensity, half the ground motions produce a hinge rotation beyond the yield limit in the longitudinal direction and some of them exceed this threshold for both directions. Thus, nonlinear behavior in the columns occurs for 15 of 30 ground motions for beyond design intensity. However, the mean ductility demand is 1.7 and the maximum value observed is 4.6, indicating that the deformation in the column is limited and does not increase to the point of likely collapse.

The maximum bearing shear strains are shown in Figure 4.7 for all the simulations. For the design level intensity, the bearing shear strain remains below 300%, with 7 ground motions exceeding a shear strain larger than 250%, after which hardening can show up based on the model. At the higher intensity, half of the ground motions produce a shear strain beyond 250% for the bearings

located at the bents and larger than 300% for bearings at the abutments. The maximum shear strain response per direction can be observed in Figure 4.8 indicating a notable difference between the maximum strain of abutment bearings and bent bearings in the longitudinal direction. The increase in shear strain is on average a factor of 1.37 in because the bents act as a cantilever in the longitudinal direction are more flexible.

4.2 MODIFICATION TO THE SEISMIC ISOLATION SYSTEM

In the previous section, the bridge response considering the original design was evaluated under design level and beyond-design level ground motions showing the potential for damage under stronger shaking. Two modifications to the design of the isolation system are considered to examine potential improvements in the bridge performance considering for beyond-design shaking. The first design modification considers different redistribution of properties for the seismic isolation bearings while the second adds supplemental viscous damping.

4.2.1 Alternative design: Bearing configuration

In the first modification to the design, the primary objective is to minimize the damage to the bridge bent by redistributing the stiffness of the bearings. This is achieved by reducing the height of rubber in the LRB at the abutment to make it stiffer. In addition, the rubber shear strain increases for a given displacement, causing the bearing response to engage hardening earlier. This modification can potentially reduce displacements, especially when considering beyond-design response. Conversely, the rubber height is increased at the bent bearing to decrease the shear strain for the same deck displacement and transfer a smaller shear force to the columns. The diameter of the bearings and lead plug insert remain unmodified to maintain similar axial pressure on the rubber. Nevertheless, despite these changes, the overall design properties of the bridge are similar when considering the linear effective properties of the isolation system and expected design displacement. Note that deck displacement can also be limited by adding restrainers in the transverse direction. However, the abovementioned adjustment is explored as a simple alternative.

To provide more details regarding the bearing modifications and the resulting model properties, the number of rubber layers at the abutment is reduced from 26 to 20 while maintaining the same layer rubber thickness of 7 mm. By implementing this modification, abutment bearings would have a shear strain of 238% for the design displacement, and 381% for the gap distance (clearance with the abutment), which is 53.3 cm (21.0 inches). To maintain the same linear effective properties of the isolation system, the number of rubber layers at the bent bearings were increased from 26 to 37 layers of 7 mm thickness. Although the effective linear properties remain the same, more advanced bearing models are expected to engage hardening for smaller deck displacements at the abutment while the bent bearings transfer less force to the columns.

It should be noted that this design increases the slenderness of the bearing at the bent. Assuming the average maximum bearing displacement from the time-history analyses, this design satisfies stability requirements. Nevertheless, a more comprehensive analysis is needed to fully evaluate the stability of this overall configuration, which is beyond the scope of this study.

4.2.2 Alternative design: Supplemental viscous damping

The second design modification adds supplemental viscous dampers between the abutments and the deck. The arrangement of viscous dampers is shown in Figure 4.9. The selection of supplemental viscous damping ratio is based on limiting the nonlinear behavior at the columns. As mentioned before, a hinge rotation of 2e-3 is considered as the yield limit in the longitudinal direction. The time-history analyses indicate that a deformation of this magnitude occurs when the deck displacement is 45 cm. Therefore, this value is set as the target deck displacement for the required supplemental damping ratio.

The original bridge subjected to beyond design shaking has an average displacement of the deck in the longitudinal direction of 42 cm and the median plus one standard deviation (x+σ) is equal to 56 cm. To reduce this displacement to the target value of 45 cm, a damping reduction factor of 1.24 is required. This is demonstrated graphically in Figure 4.10.

The total effective damping is considered as the sum of the effective damping provided by the isolation system plus the damping provided by the viscous dampers:

$$\xi_{eff} = \xi_{iso} + \xi_{dampers}$$

The effective damping ratio provided by the isolation system, ξ_{iso}, associated with 56 cm is equal to 22.4%. Using the formula provided by AASHTO (2020), such damping ratio gives a current reduction factor of B_M:

$$B_M^{current} = \left(\frac{\xi_{eff}}{0.05}\right)^{0.3} = \left(\frac{0.224}{0.05}\right)^{0.3} = 1.57$$

Then, the total required reduction can be defined as:

$$B_M^{required} = 1.24 B_M^{current} = 1.95$$

Finally, the required damping provided only by the viscous dampers can be computed from:

$$B_M^{required} = \left(\frac{\xi_{iso} + \xi_{dampers}}{0.05}\right)^{0.3} = 1.95$$

Following this approach, the total damping ratio of 46.4% is required to reduce the displacement to the target value, which means a damping provided by the viscous dampers of $\xi_{dampers}$ equal to 24%. The damping ratio provided by the viscous dampers was set equal to 25% in the model.

AASHTO limits the effective damping to 30% for using equivalent linear static design procedures due to the lack of reliability of the reduction factor B_M. In this study the total damping provided by the isolation system plus the viscous dampers exceeds this limit, however, nonlinear time-history analysis is used in this study.

4.3 STRUCTURAL RESPONSE

The structural response of the bridge is examined and compared for the original design and the two design modifications under beyond-design level ground motions. The orbital response of the three configurations subjected to Record 24 are shown in Figure 4.11. The original and stiffening configuration have similar deck displacements as expected, however, there are two impacts for the original design and only one for the stiffening configuration. The configuration including dampers has a significant reduction of the deck displacements with no impacts. This is a much more effective approach though it requires additional hardware.

Figure 4.12 shows the bearing hysteresis in the longitudinal direction for the abutment and bent bearings of the three configurations. The original isolation design produces a maximum shear strain of about 300% in the abutment bearing (Figure 4.12a) while reaching 400% in the shorter bearings (Figure 4.12c) and having significant hardening behavior. The modified bent bearing (Figure 4.12d) has a much smaller shear strain and lower forces to protect the bent. The design with dampers shows to be an effective approach to reduce displacement demand for all the bearings.

It is important to note that under 2D horizontal excitation, bearings may have significant shear strain in both directions. Hardening in the bearing hysteresis can show up at smaller strains in the longitudinal or transverse direction because the radial shear strain may be large. Figure 4.13a shows the hysteresis loop of the bent bearing for "stiffening configuration" rotated to 145º corresponding to the maximum deformation. Figure 4.13b shows the orbital shear strain versus orbital shear force. From both plots, the actual shear strain exceeds 400%, resulting in significant hardening previously observed in the longitudinal and transverse response. It should be noted that the bearing model was calibrated with experimental data up to 400% shear strain and beyond this range the bearing behavior is not well known with potential risk of failure.

The column hinge responses for the three configurations are shown in Figure 4.14. Both design modifications were effective in reducing the nonlinear behavior of the bent, with the added dampers again having the most significant benefits.

For Record 24, there was one impact at each abutment backwall for the original design, and one impact at the west abutment with modified bearings. Figure 4.15 shows the contact force-indentation curves for these impacts. The deformation sign was changed depending on the

abutment location for easier interpretation. The impact forces range was between 60% to 100% of the deck weight.

Figure 4.16 shows the force-deformation curve for the backfill soil. The soil undergoes a maximum deformation of 30 mm, sustaining between 12% to 16% of the deck weight. The bridge serviceability may be compromised due to the soil residual deformation behind the backwall. The backwall force-deformation behavior is shown in Figure 4.17 for the different instances of impact. The brittle behavior of the wall failing in shear produces a peak force during the first few millimeters of deformation, followed by a decline in capacity. After this point, the resisting force is purely provided by the backfill soil of the abutment.

It is important to point out that in all the impact cases examined in this study, the abutment backwall failed. There were no records for which a low velocity impact occurred, and the wall remained elastic or with low damage. This is acceptable since the backwall is considered sacrificial with the ability for rapid repair though mitigation strategies can be beneficial to enhance the backwall performance and immediate serviceability of the bridge.

The maximum responses for all the records scaled to the beyond-design seismic hazard are examined next for the three bridge configurations. The numbering of the ground motions is maintained the same as in the previous section and are sorted from the smallest to the largest bearing displacement for the original design.

Figure 4.18 shows the maximum orbital deck displacement for the three configurations, and the maximum deck displacements in the two horizontal directions. The abutment gap distance is also shown in Figure 4.18b. The maximum displacements for the original design and the reconfigured bearings are very similar with no difference for the smaller displacement demands. The second half of the records with the larger bearing demands show that the stiffening configuration gives slightly smaller displacements on average than the original design. Even though larger strain demands on the bearings resulted in more strain hardening in the rubber, this approach does not effectively reduce the deck displacement for this structure. The orbital bearing response for the original and stiffening configuration is illustrated in Figure 4.19, where the deformation is shown in millimeters for a better comparison. The stiffening configuration provides a peak force 35% higher compared to the force provided by the original configuration. Nevertheless, the maximum bearing displacement does not show significant variation. Alternatively, supplemental viscous dampers have a significant reduction of about 60% in the maximum displacement compared to the original design.

The maximum column hinge rotation for the three bridge configurations is shown in Figure 4.20. An effective reduction in the rotation demand for the two modified designs is observed when compared to the original design. The damping configuration gives the smallest rotations in the longitudinal direction, while both modifications provide similar reductions for the transverse direction. Moreover, Figure 4.21 shows the fraction of the total deck displacement due to the bent deformation in the longitudinal direction versus the column hinge rotation. From this data, it can be observed for hinge rotations just above the yield limit, the bent deformations contribute to about

20-25% of the total deck displacement. As the columns yield and hinge rotation increase, the bent contribution to deck displacement increases from about 22% to 35%. This indicates that when bent column yields, the effectiveness of the isolation system is reduced though that shift is gradual, and the isolation system maintains a large portion of the displacement demands.

Figure 4.22 shows the maximum shear strain deformation in the rubber bearings for the three bridge configurations. There is a reduction in the shear strain demand for the taller bearings on the bent when compared with the original design. However, the shear strain demand increases significantly for abutment bearings, with about half the records having shear strains larger than 400%. Among those instances, four records had shear strain deformation larger than 500%, which can be assumed as failure of the bearings with the potential for unseating. The original design gives smaller shear strain demands at the abutment with four records having a shear strain deformation larger than 400% and only one record exceeding 500%. Note that this configuration was a trial and future studies can look at optimizing this design to have lower shear strains. The configuration with dampers is able to maintain shear deformations at a maximum of about 300% shear strain for all the records.

Considering the effects of impact, the maximum deformation of the abutment backfill soil is shown in Figure 4.23. The overall trend of soil deformation is similar for both the stiffening configuration and the original case. According to Wilson and Elgamal (2010), the maximum load capacity of the soil can be reached at a deformation of about 0.027-0.03 times the wall height, after which the soil starts to lose strength, while the ultimate deformation can be achieved at around 8% of the wall height. For this prototype bridge, 3% of the heigh is equivalent to about 55 mm, which is exceeded in one ground motion for the original design, and three cases for stiffening configuration. The ultimate deformation of 8%, equivalent to 146 mm, is not exceeded for any of the simulations conducted. However, for ground motion 29, the abutment bearings reached 500% shear strain at which failure is likely to occur and the numerical model was unstable. Prior to this issue, the abutment backfill soil had a deformation of 73mm.

Table 4.1 summarizes key parameters related to the overall performance of the bridge considering the three design configurations. The number of records that produced at least one impact indicates a failure in the abutment wall that would require repair. The total impacts further note the potential for severity of the damage in the abutment and the deck. The following parameter identifies the number of records with an abutment-bearing shear strain greater than 400%. From the literature, it can be presumed that values over 400% are close to the failure of the bearing (Kikuchi et al. 2010 Yamamoto et al. 2008; Marquez 2021). Bearing failure was explicitly assumed to be at 500% shear strain for these simulations to extend the range over which the bridge behavior can be observed. As mentioned above, a backfill soil deformation of 55 mm can be defined as limit state indicating the maximum load capacity of the soil. Finally, related to column damage assessment, a hinge rotation for longitudinal deck motion equal to 0.2% radians is defined as a threshold for a nonlinear behavior at the bent.

CHAPTER 4: TABLES

Table 4.1 Summary of performance parameters

Variable	Original Design	Hardening Design	Damping Design
Records with at least one impact	11	9	0
Total impacts	21	15	0
Records with bearing shear strain larger than 400%	4	15	0
Maximum soil deformation larger than 3%hw (55mm)	1	3	0
Hinge rotation (Longitudinal direction) greater than 0.2% rad	15	9	3

CHAPTER 4: FIGURES

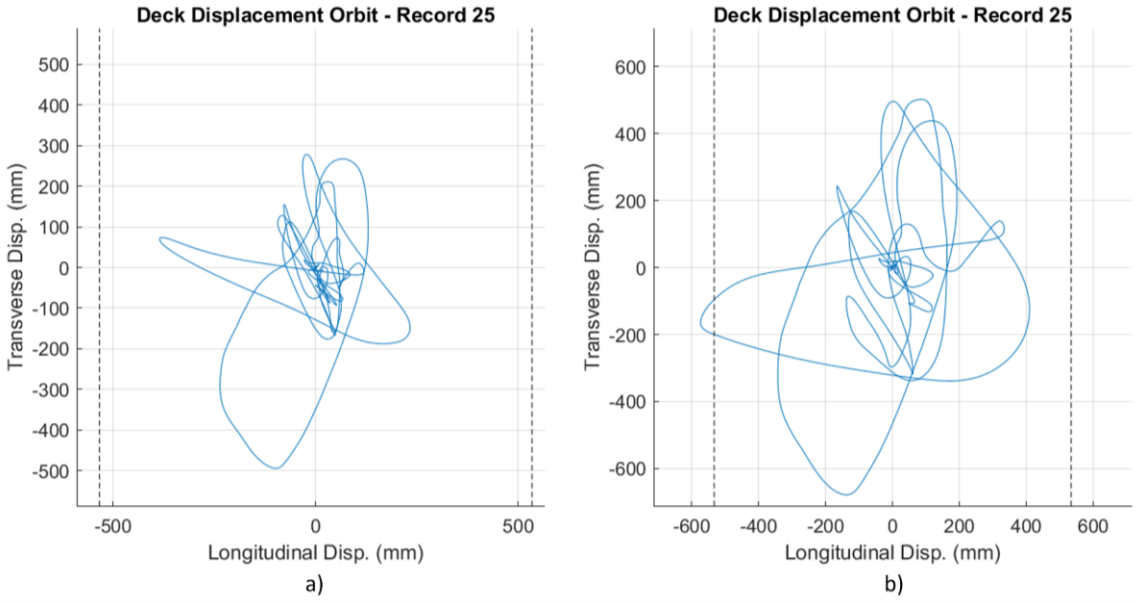

Figure 4.1 **Orbit deck displacement for record 25: a) Design level (975 years of return period); b) Beyond-design level (2475 years of return period)**

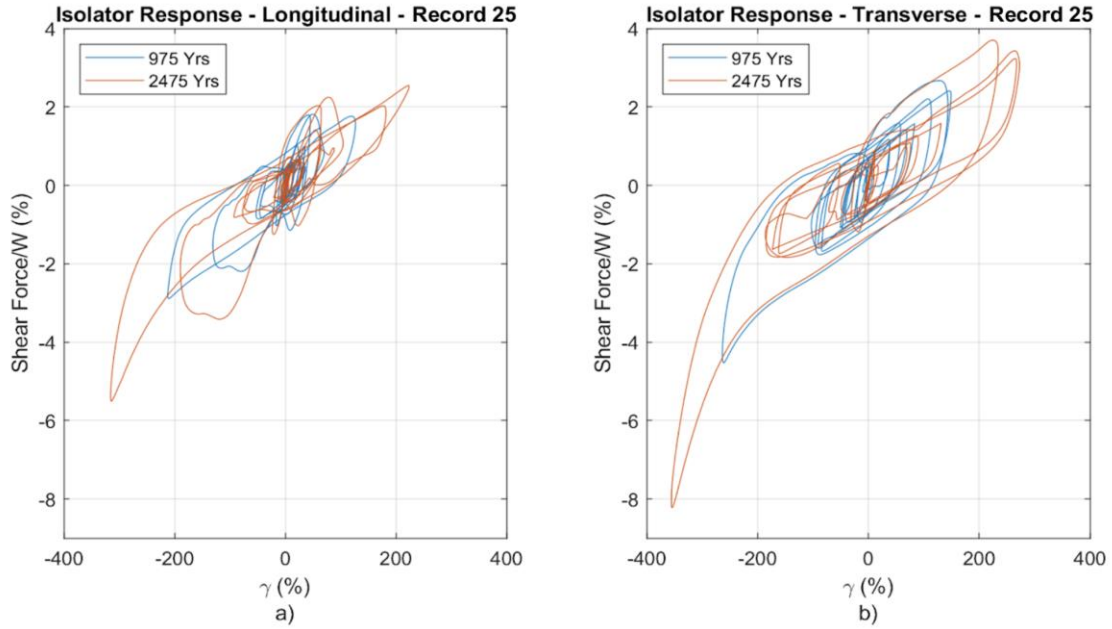

Figure 4.2 **Abutment bearing hysteresis for record 25 at design (975 yr) and beyond-design level (2475 yr): a) Longitudinal direction; b) Transverse direction**

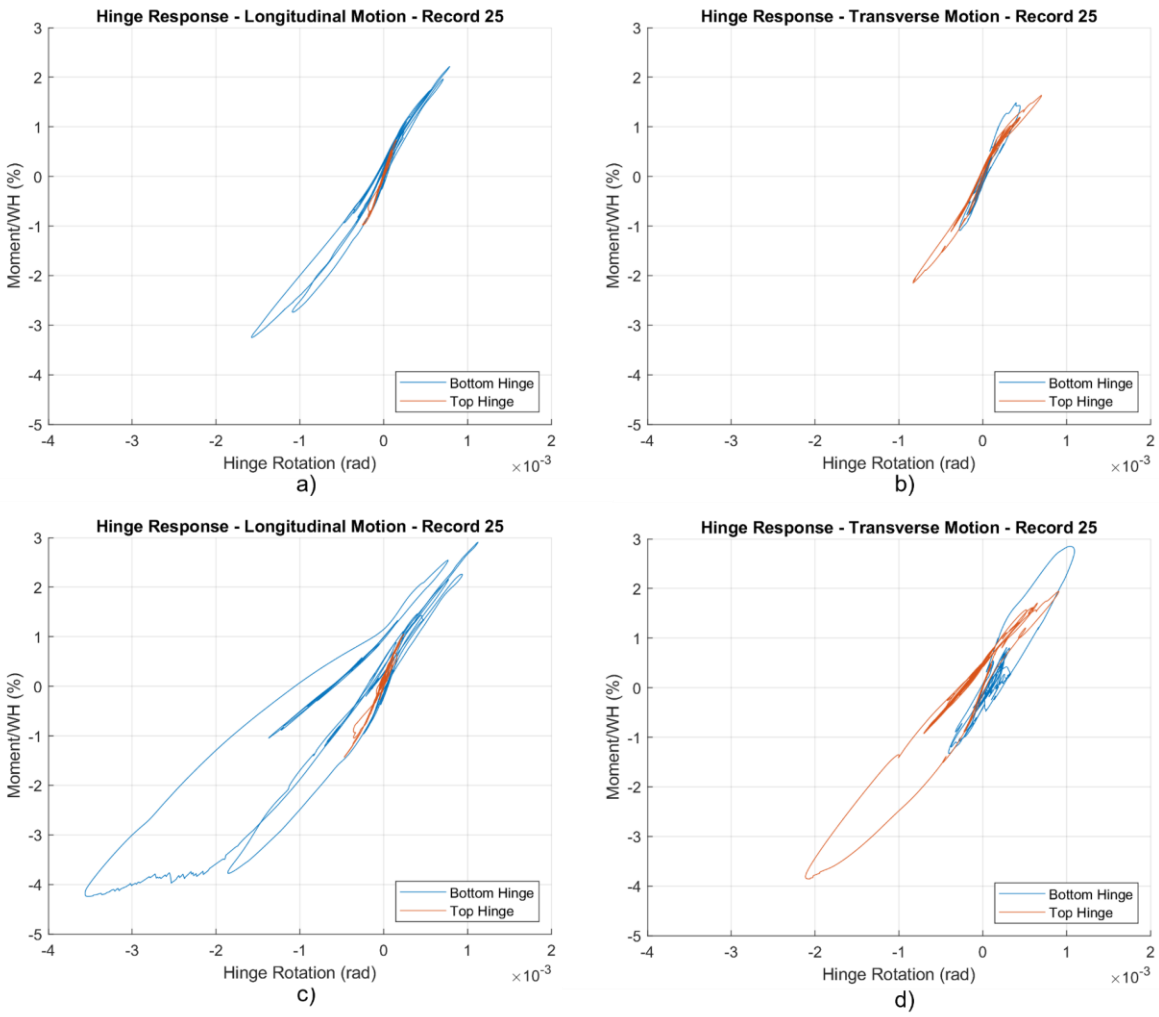

Figure 4.3 Column hinge hysteresis for record 25: a) Longitudinal motion - design level; b) Transverse motion - design level; c) Longitudinal motion - beyond-design level; d) Transverse motion - beyond-design level

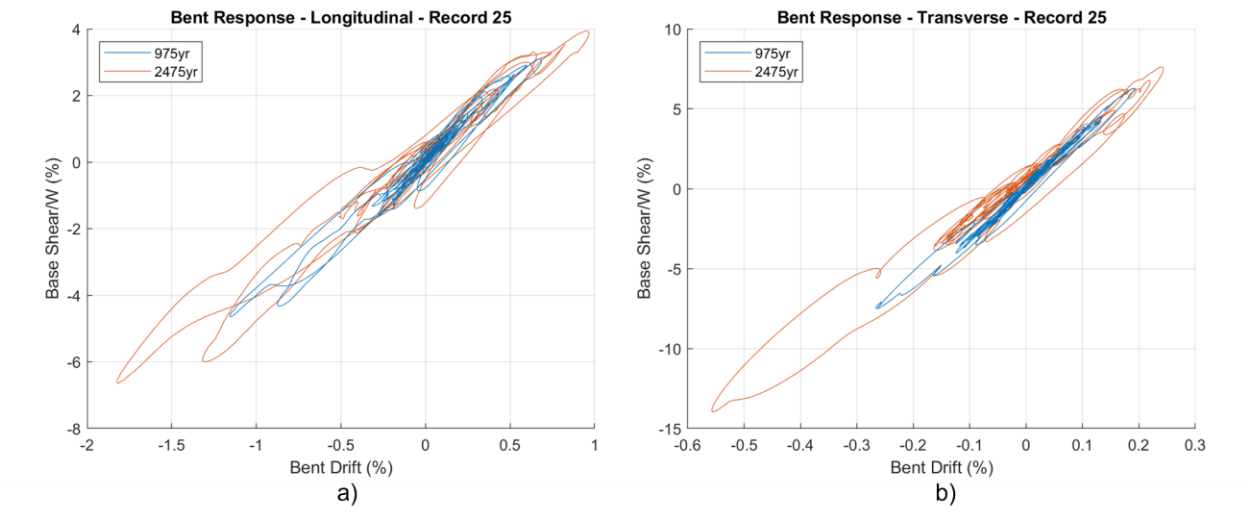

Figure 4.4 Bent response for record 25 for design (975yr) and beyond-design level (2475yr): a) Longitudinal direction; b) Transverse direction

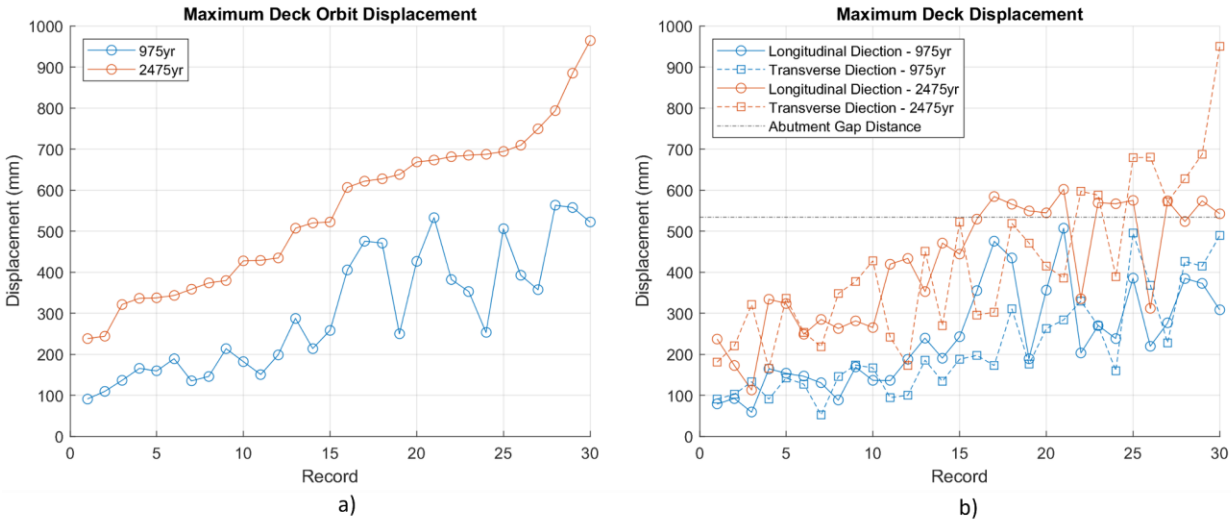

Figure 4.5 Maximum deck displacement for design (975yr) and beyond-design level (2475yr): a) Orbital displacement; b) Displacement per direction

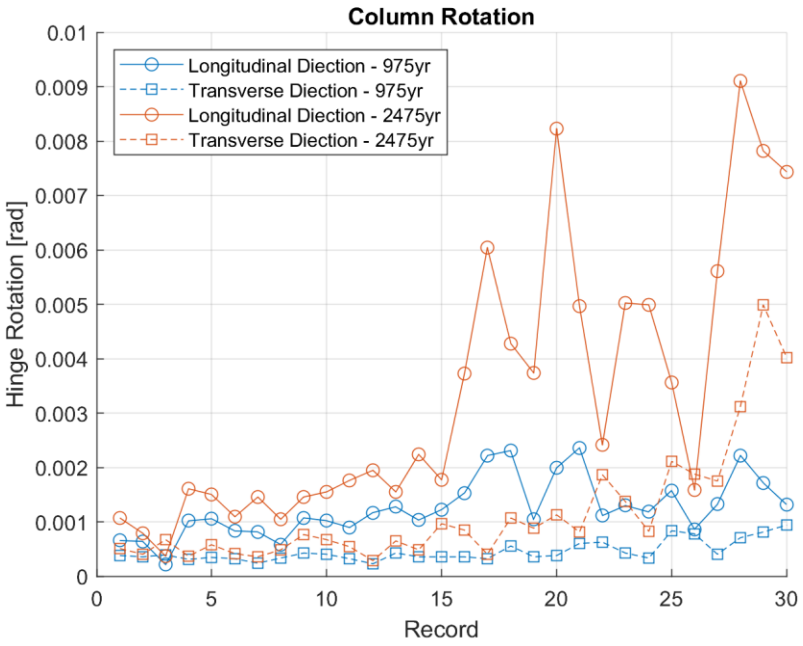

Figure 4.6 Maximum column hinge rotation for design (975yr) and beyond-design level (2475yr)

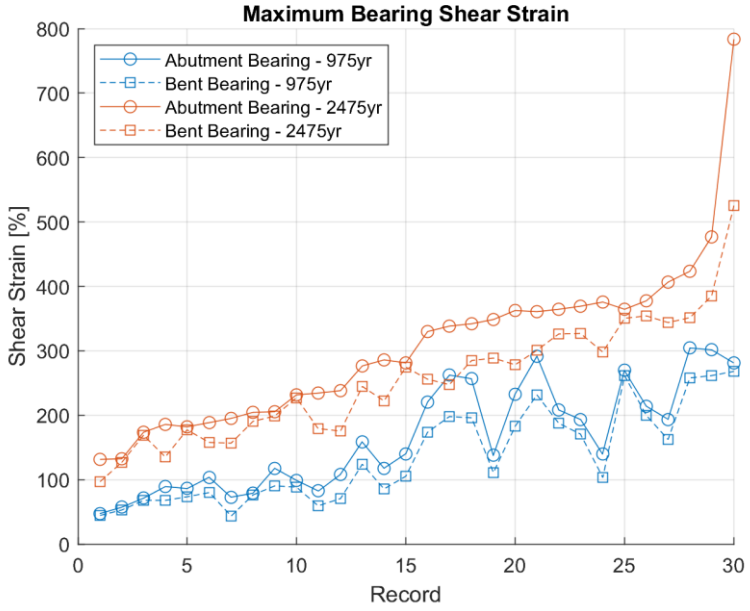

Figure 4.7 Maximum bearing shear strain for design (975yr) and beyond-design level (2475yr)

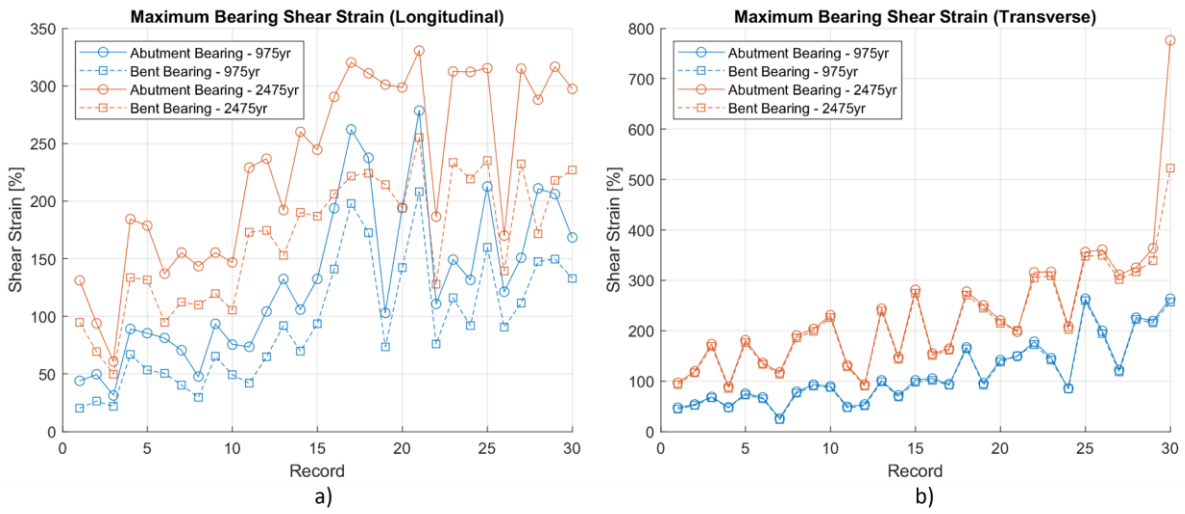

Figure 4.8 Maximum bearing orthogonal shear strain for design (975yr) and beyond-design level (2475yr): a) Longitudinal direction; b) Transverse direction

Figure 4.9 Plan view of viscous dampers location

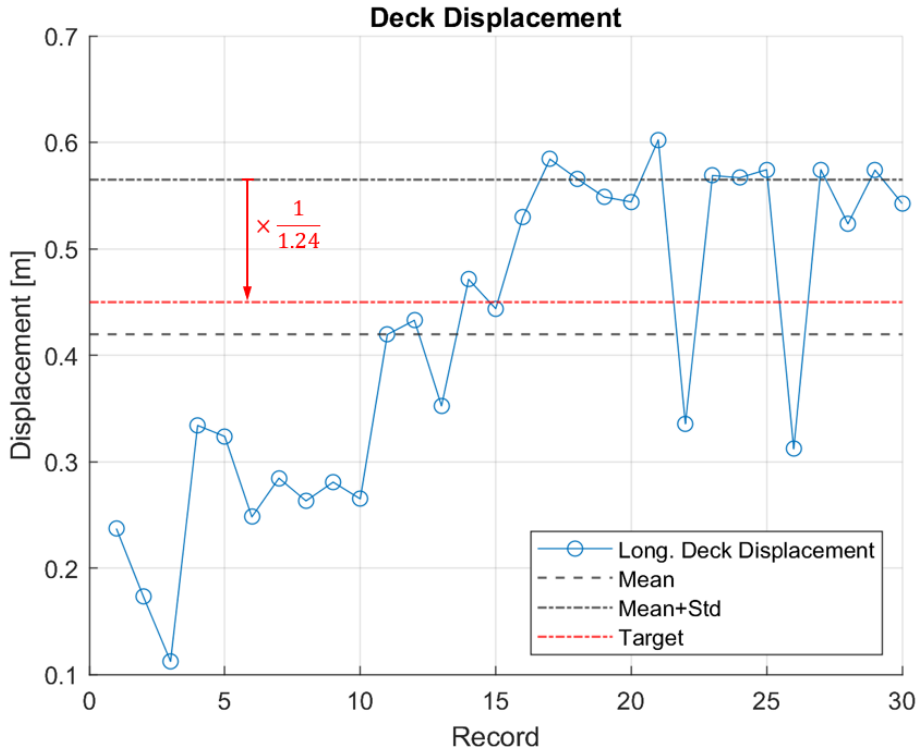

Figure 4.10 Maximum longitudinal deck displacement for beyond-design level

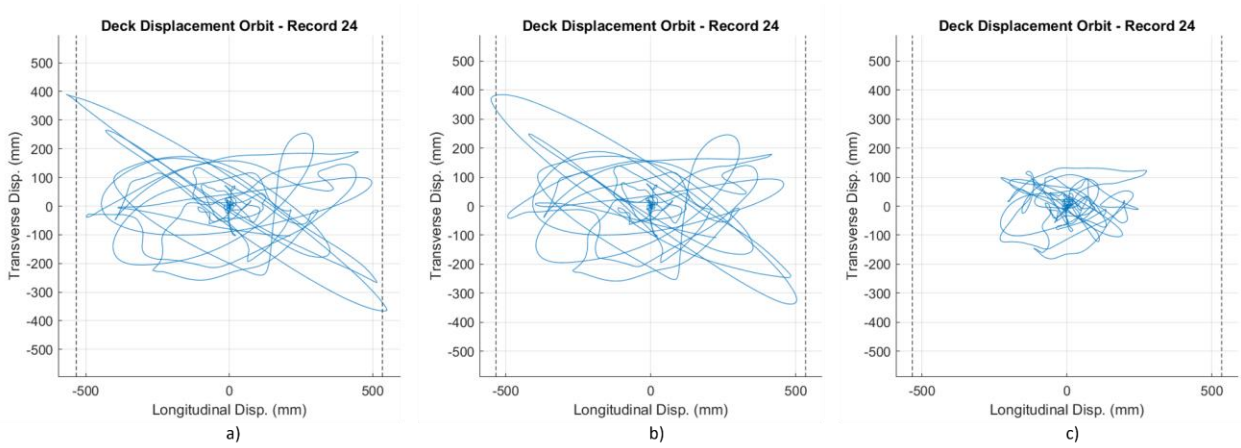

Figure 4.11 Orbital deck displacement for record 24 for: a) Original design; b) Stiffening configuration; c) Damping configuration

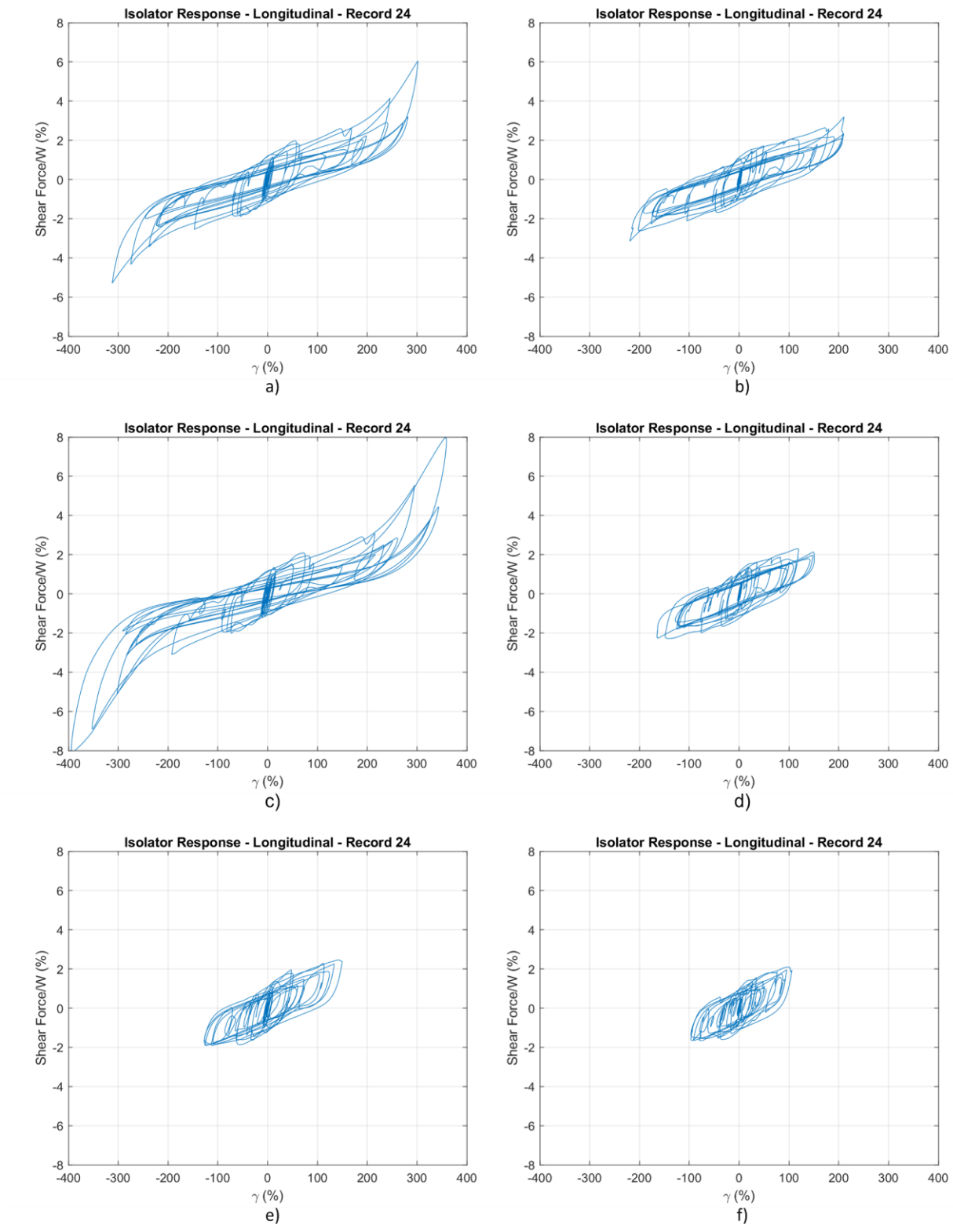

Figure 4.12 Bearing hysteresis for record 24: a) Original design, abutment; b) Original design, bent; c) Stiffening configuration, abutment; d) Stiffening configuration, bent; e) Damping configuration, abutment; f) Damping configuration, bent

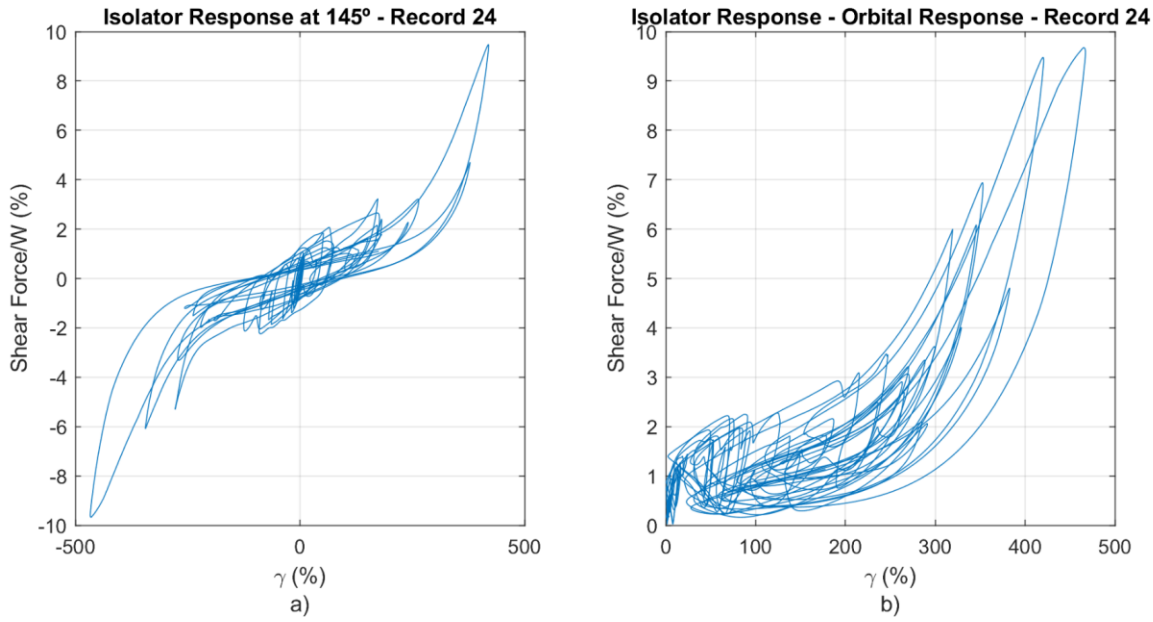

Figure 4.13 Maximum bearing response for stiffening configuration: a) Hysteresis rotated 145º; b) Orbital response

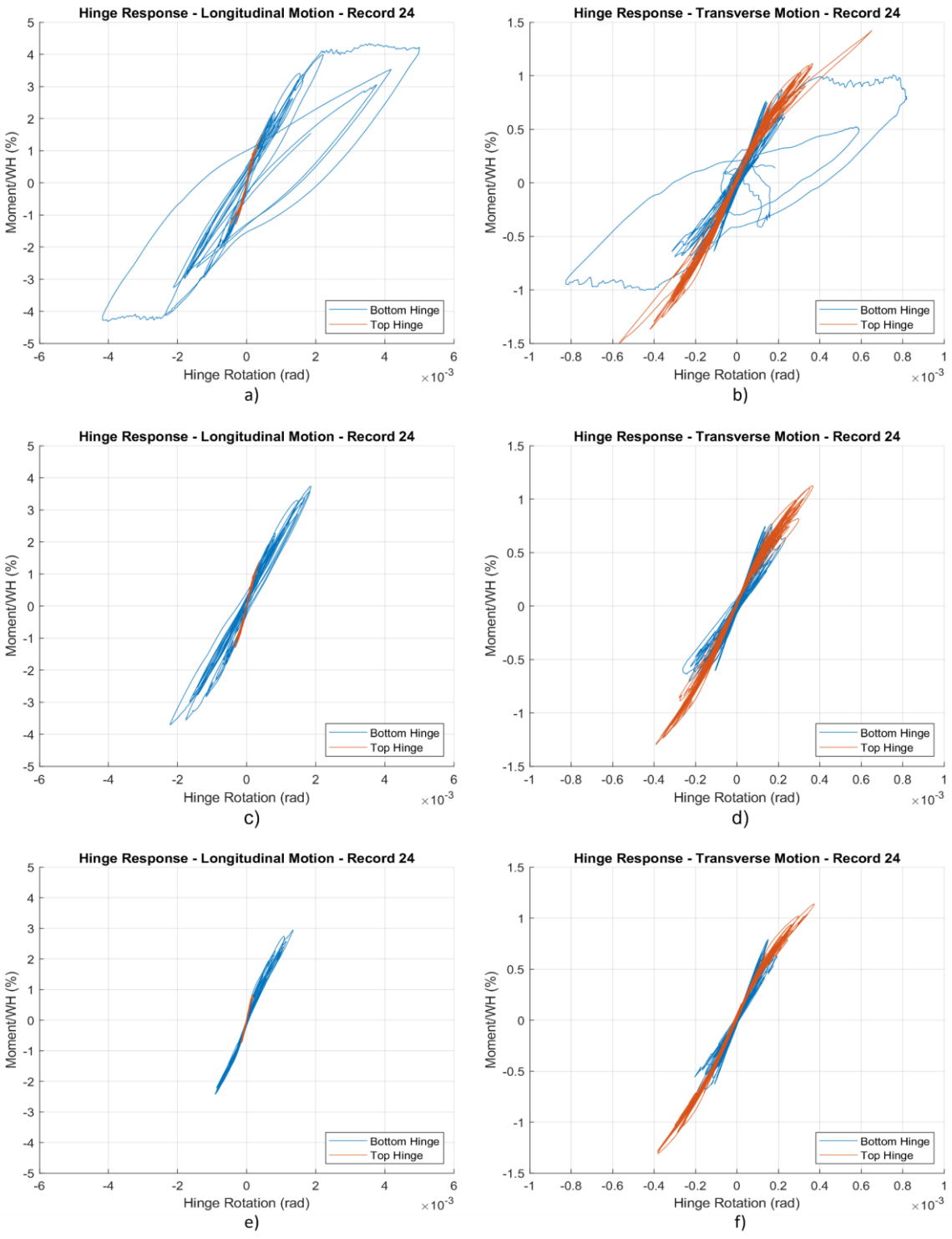

Figure 4.14 Column hinge hysteresis for record 24: a) Original design, longitudinal; b) Original design, transverse; c) Stiffening configuration, longitudinal; d) Stiffening configuration, transverse; e) Damping configuration, longitudinal; f) Damping configuration, transverse

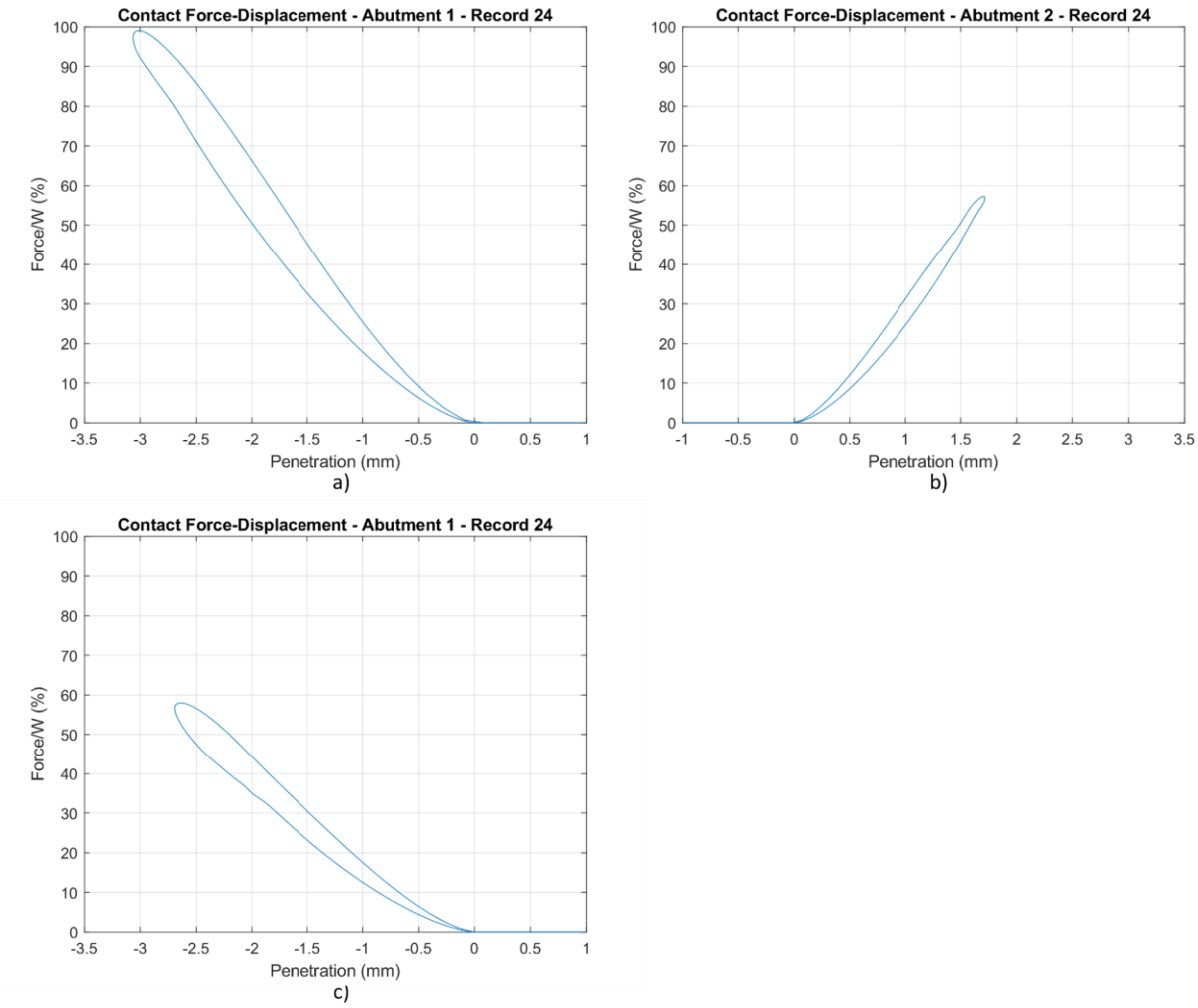

Figure 4.15 Total contact force-indentation curve for record 24: a) Original design, abutment 1; b) Original design, abutment 2; c) Stiffening configuration, abutment 1

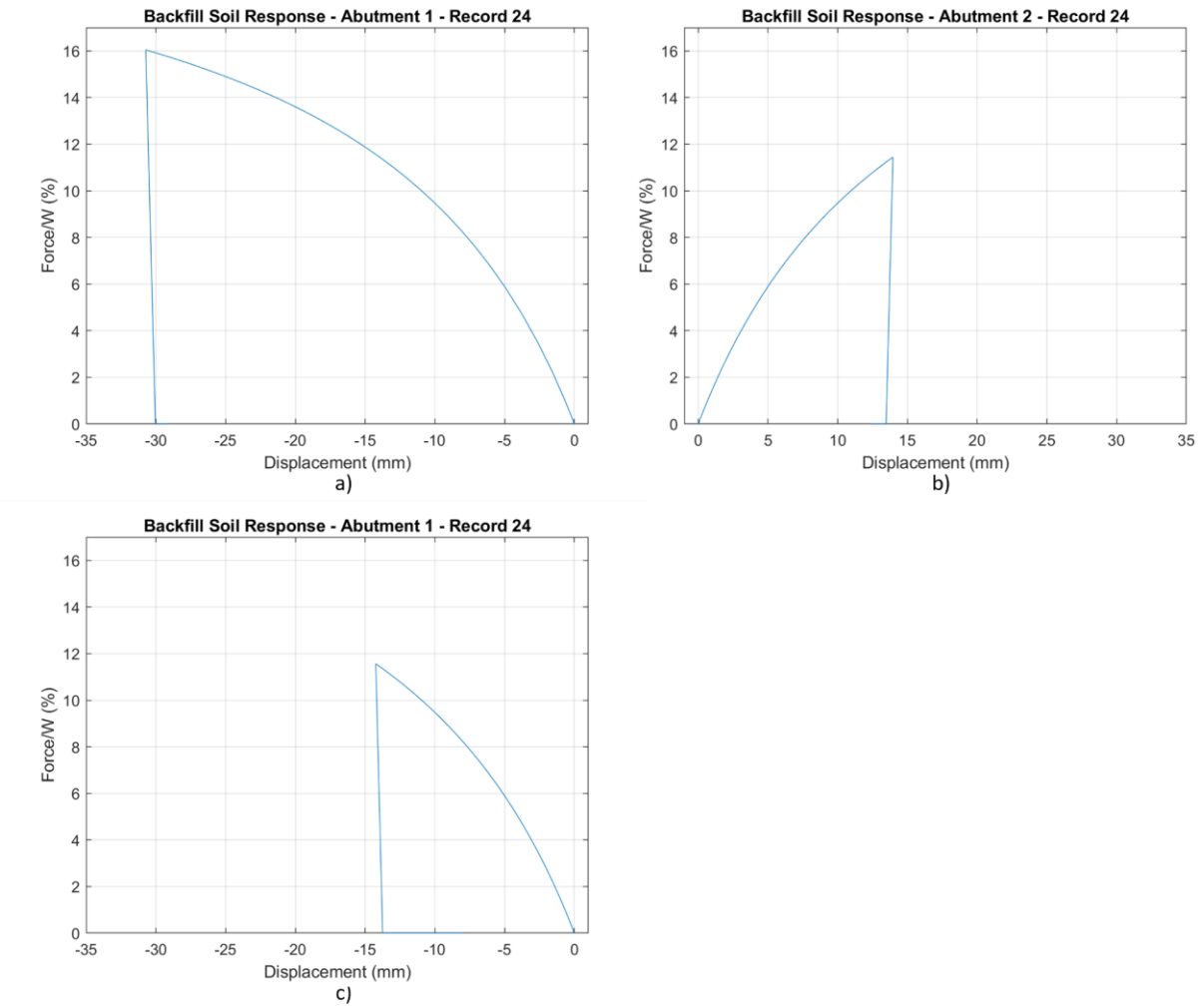

Figure 4.16 Backfill soil force-deformation curve for record 24: a) Original design, abutment 1; b) Original design, abutment 2; c) Stiffening configuration, abutment 1

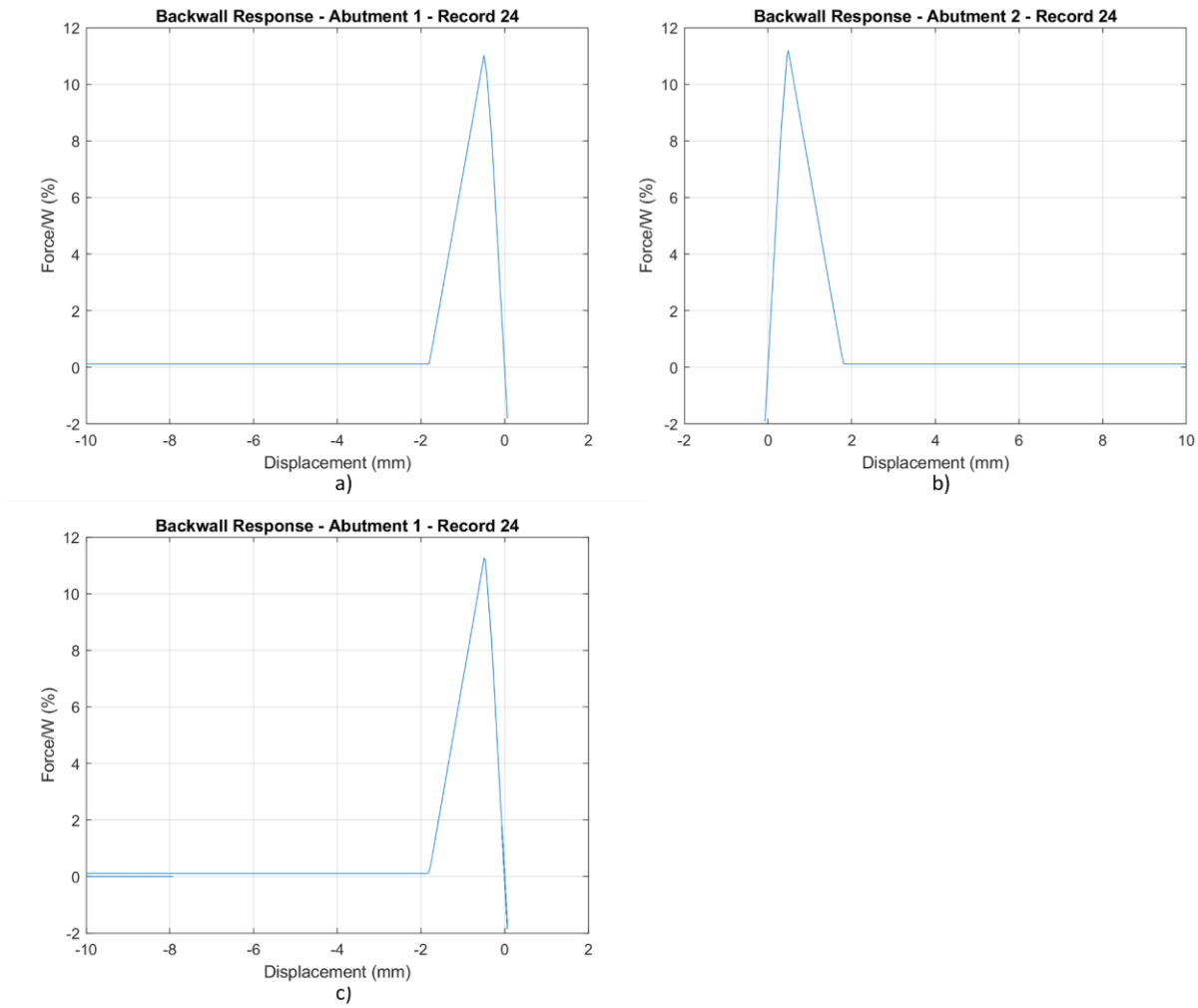

Figure 4.17 Abutment backwall force-deformation curve for record 24: a) Original design, abutment 1; b) Original design, abutment 2; c) Stiffening configuration, abutment 1

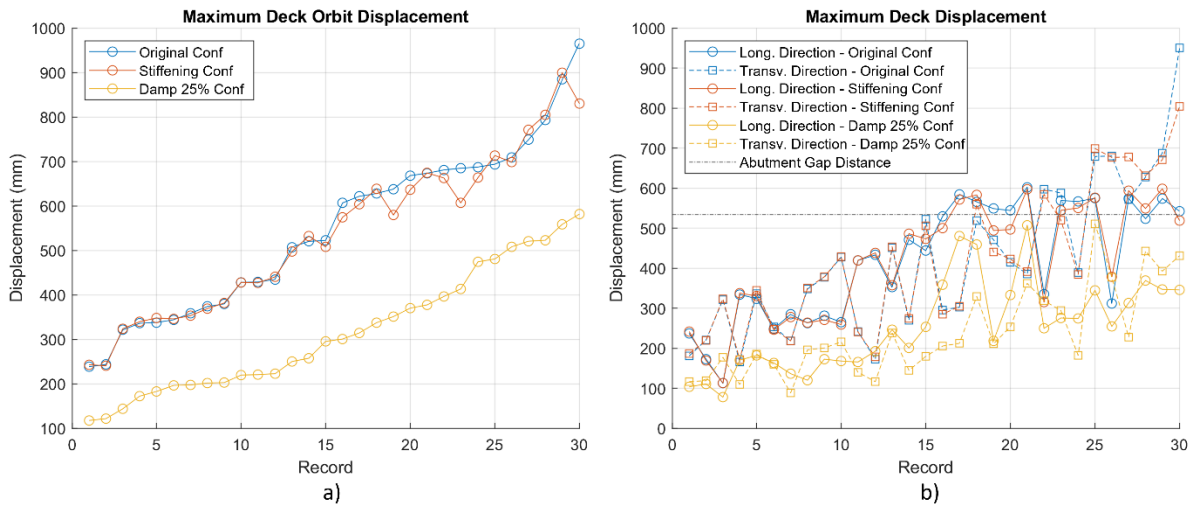

Figure 4.18 Maximum deck displacement for the three cases: a) Orbital; b) Orthogonal

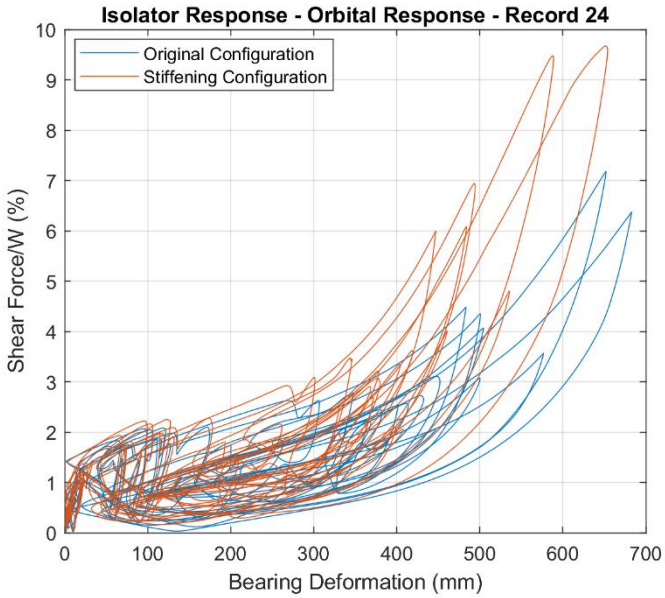

Figure 4.19 Orbital bearing response for original and stiffening configuration

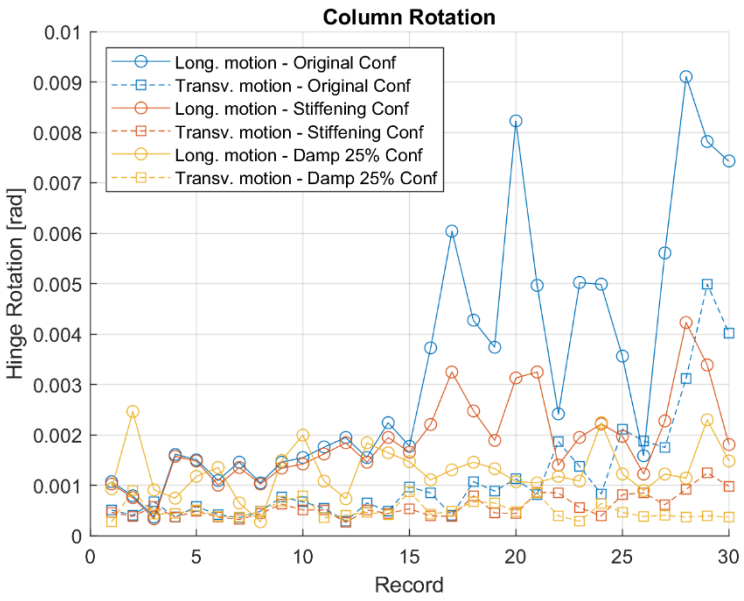

Figure 4.20 Maximum column hinge rotation for the three cases

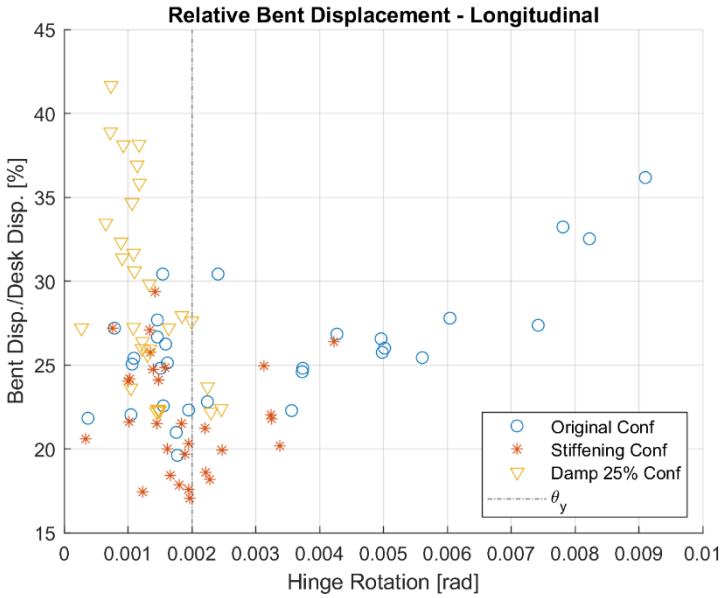

Figure 4.21 Relative bent deformation respect to the deck displacement for the three cases

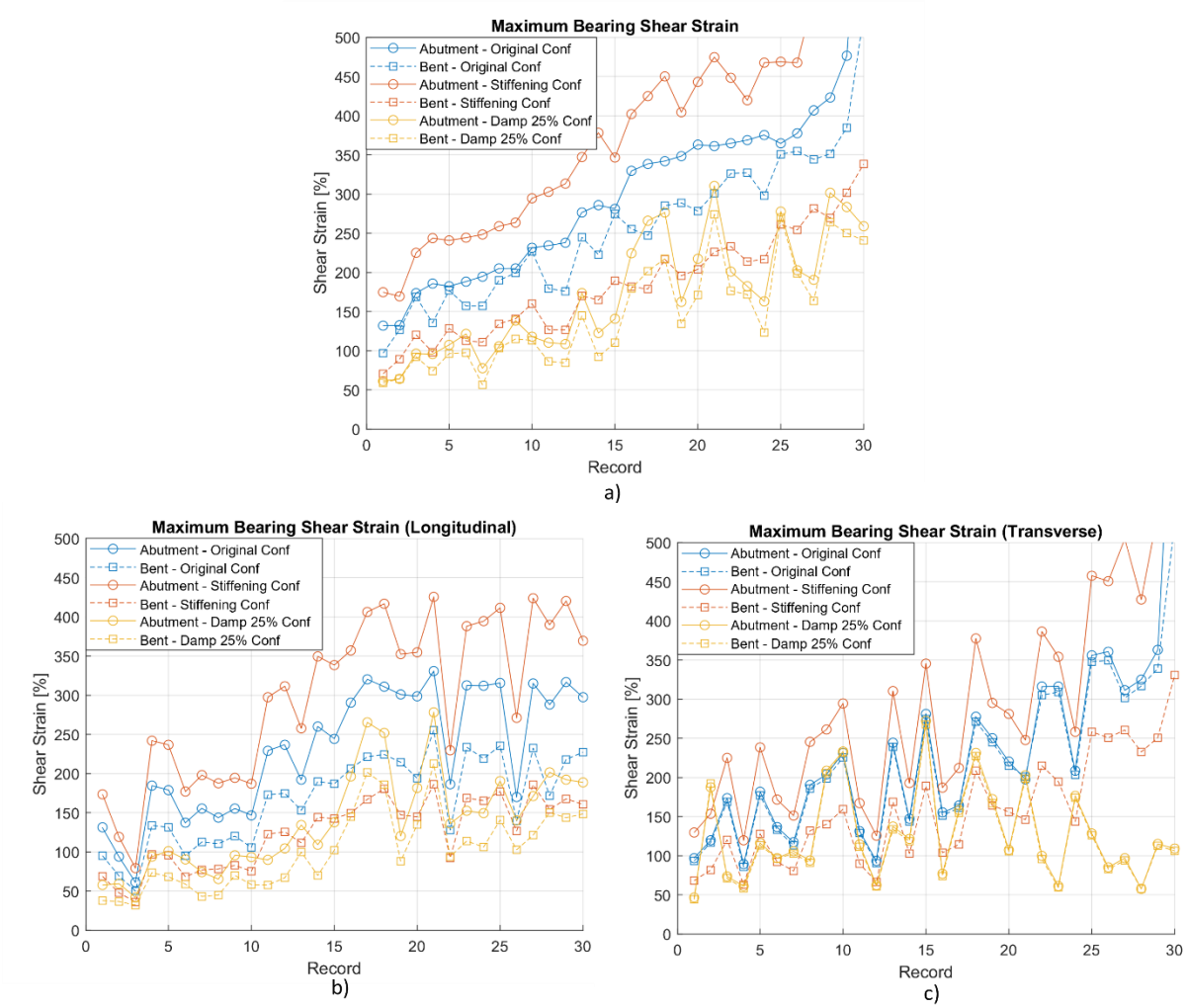

Figure 4.22 Maximum bearing shear strain for the three cases: a) Orbital; b) Longitudinal; c) Transverse

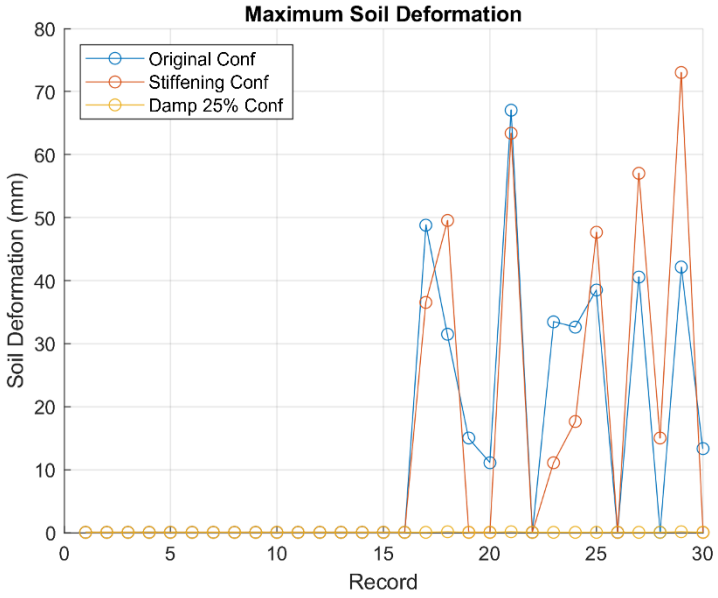

Figure 4.23 Maximum soil deformation for the three cases

5 CONCLUSIONS

5.1 SUMMARY

This study assesses the performance of a seismically isolated bridge under design-level and beyond-design level ground shaking. While minimal damage if any can be expected under design level shaking, an increased seismic hazard is considered to evaluate the expected progress of damage and potential failure modes of the bridge which are largely unknown. In an effort to further enhance the safety and performance of seismically isolated bridges, two different modifications to the seismic isolation system are examined. It is important to note that this preliminary study and the following conclusions are based on observations of a single bridge model and more extensive studies are required to fully understand the expected behavior of bridges under beyond design shaking.

Considering design-level shaking, the isolated bridge shows adequate performance as expected, with limited nonlinear behavior at the columns, no pounding against the abutments and the maximum shear strain in lead rubber bearings remains within capacity at or below 300%.

For the beyond design-level seismic hazard, the displacement demands on the isolation system are about twice as large compared to the design-level ground motions. This increase in displacement results in 11 of 30 ground motion pairs causing pounding between the deck and abutment. A simplified model of the abutment backwall and backfill soil was developed and indicated the potential for backwall failure in shear, and significant permanent deformations but did not achieve the peak strength and full failure of the soil.

The increased demands on the isolation system result in larger shear forces that can yield the supporting bents, especially in the longitudinal direction. The column moment-rotation behavior shows significant yielding though ductility was limited and did not achieve the onset of strength degradation that was incorporated in the plastic hinge model. As the columns yield, their relative contribution to the deck displacement increases, reducing the effectiveness of the isolation system. Nevertheless, bearings still absorbed most of the deck displacement demands. This behavior is expected and considered in the current design guidelines although it has not been studied in detail with nonlinear analyses. Further experimental and numerical studies are required to better understand the interaction and distribution of nonlinear behavior between the bearings and the columns.

Regarding shear strain at the bearings, 4 out of 30 ground motions produced a deformation greater than 400% without restraints in the lateral direction, which raises concerns regarding a potential limit for bearing failure. Overall, the results indicate that the failure mode for a seismically isolated bridge under beyond design shaking is likely bearing failure in the transverse direction with potential of unseating of the deck.

5.2 SUMMARY

In order to improve the performance of the isolated bridge, two different alternatives were analyzed: The first one consists of changing the bearing configuration in order to reduce the forces transferred to the bent and engage hardening at the abutment bearings at early stages. This option proved to be effective in reducing the force demands of the bent, while reductions in the deck displacements were negligible. Shear strain at the abutment bearings increased compared with the original design with a potential for failure. A more detailed design in future studies can examine if these deficiencies can be overcome in the proposed modification that does not require additional hardware.

Supplemental viscous dampers were also considered for the seismically isolated bridge. Targeting 25% additional damping ratio, all the performance parameters observed were significantly improved. No abutment pounding and limited nonlinear behavior at the columns were observed. However, the abutment and its foundation need to be considered for the damper forces, which was beyond the scope of this study.

REFERENCES[2]

AASHTO (2020). AASHTO LRFD Bridge Design Specifications, 9th ed., The American Association of State Highway and Transportation Officials, Washington DC.

Ancheta T.D., Darragh R.B., Stewart J.P., Seyhan E., Silva W.J., Chiou B.S.J., Wooddell K.E., Graves R.W., Kottke M.A.R., Boore D.M., Kishida T., Donahue J.L. (2012). NGA-West2 Database, Earthq. Spec., 30(3):989-1005, doi:10.1193/070913EQS197M

ASCE (2017). *Minimum design loads and associated criteria for buildings and other structures*, ASCE 7-16, Reston, VA.

Aviram A., Mackie K.R., Stojadinović B. (2008). Guidelines for Nonlinear Analysis of Bridge Structures in California, PEER Report No. 2008/03, Pacific Earthquake Engineering Research Center, University of California, Berkeley, CA.

Baker J.W., Lee C. (2018). An Improved Algorithm for Selecting Ground Motions to Match a Conditional Spectrum, J. Earthq. Eng., 22(4):708–23, doi.org/10.1080/13632469.2016.1264334.

Baker J.W. (2011). Conditional Mean Spectrum: Tool for Ground-Motion Selection, J. Struct. Eng., 137(3):322–31, doi.org/10.1061/(asce)st.1943-541x.0000215.

Baker J.W., Lin T., Shahi S.K. (2011). New Ground Motion Selection Procedures and Selected Motions for the PEER Transportation Research Program, PEER Report No. 2011/03, Pacific Earthquake Engineering Research Center, University of California, Berkeley, CA.

Buckle I.G., Al-Ani M., Monzon E. (2011). *Seismic Isolation Design Examples of Highway Bridges*, Tech. rep. NCHRP Project 20-7/Task 262(M2), National Cooperative Highway Research Program, Washington, DC

Buckle, I.G., Constantinou M.C., Dicleli M., Ghasemi H. (2006). Seismic Isolation of Highway Bridges, Tech. Rep. MCEER-06-SP07, MCEER, Buffalo, NY

Buckle I.G., Douglas B., Mayes R., Nutt R., Thoman S. (1994). The Northridge, California Earthquake of January 17, 1994: Performance of Highway Bridges, Tech. Rep. NCEER-94-0008, MCEER, Buffalo, NY

Caltrans. (2019a). *Seismic Design Criteria 2.0*, California Dept. of Transportation, Sacramento, CA

Caltrans. (2019b). *Seismic Design of Ordinary Bridges with Isolation Bearings*, California Dept. of Transportation, Sacramento, CA

Chang G.A., Mander J.B. (1994). Seismic Energy Based Fatigue Damage Analysis of Bridge Columns: Part I - Evaluation of Seismic Capacity, Tech. Rep. NCEER-94-0006, MCEER, Buffalo, NY

Coleman J., Spacone E. (2001). Localization Issues in Force-Based Frame Elements, J. Struct. Eng., 127(11):1257–65, doi.org/10.1061/(ASCE)0733-9445(2001)127:11(1257)

Constantinou M.C., Kalpakidis I., Filiatrault A., Ecker Lay R.A. (2011). LRFD-Based Analysis and Design Procedures for Bridge Bearings and Seismic Isolators, Tech. Rep. MCEER-11-0, MCEER, Buffalo, NY

Deb A., Zha A.L., Caamaño-Withall Z.A., Conte J.P., Restrepo J.I. (2021). Updated Probabilistic Seismic Performance Assessment Framework for Ordinary Standard Bridges in California, Earthq. Eng. Struct. Dyn. 50 (9): 2551–70. doi.org/10.1002/eqe.3459.

Deb A., Zha A.L., Caamaño-Withall Z.A., Conte J.P., Restrepo J.I. (2018). Development of Performance-Based Seismic Design of Ordinary Standard Bridges, Rep. No. CA18-2880, California. Dept. of Transportation, Sacramento, CA

DesRoches R., Muthukumar S. (2002). Effect of Pounding and Restrainers on Seismic Response of Multiple-Frame Bridges, J. Struct. Eng., 128(7):860–69, doi.org/10.1061/(asce)0733-9445(2002)128:7(860).

Domaneschi M., Martinelli L., Cattivelli C. (2018). Phenomenological Model of Rubber Bearings with Variable Axial Loading, Front. Built Env., 4(9):1–14, doi.org/10.3389/fbuil.2018.00049.

Federal Highway Administration. (2020). *National Bridge Inventory (NBI).* U.S. Department of Transportation. https://www.fhwa.dot.gov/bridge/nbi.cfm.

Feng, D., Chen C., Liu W., Tanaka K. (2004). A Performance Test Study on Chinese G4 Lead Rubber Bearings, Proceedings, 13th World Conference on Earthquake Engineering, Vancouver, Canada.

Fenz D.M., Constantinou M.C. (2008). Mechanical Behavior of Multi-Spherical Sliding Bearings, Tech. Rep. MCEER-08-0007, MCEER, Buffalo, NY

Hall J.F. (2018). Performance of Viscous Damping in Inelastic Seismic Analysis of Moment-Frame Buildings, Earthq. Eng. Struct. Dyn., 47(14):2756–76, doi.org/10.1002/eqe.3104.

Han Q., Du X., Liu J., Li Z., Li L., Zhao J. (2009). Seismic Damage of Highway Bridges during the 2008 Wenchuan Earthquake, Earthq. Eng. Eng. Vib., 8 (2):263–73, doi.org/10.1007/s11803-009-8162-0.

Hughes P. (2020). High-Fidelity and Reduced-Order Models of Contacting Structures, PhD thesis, University of California San Diego, San Diego, CA.

Hughes P.J., Mosqueda G. (2020). Evaluation of uniaxial contact models for moat wall pounding simulations, Earthq. Eng. Struct. Dyn., 49(12):1197-1215, doi.org/10.1002/eqe.3285

Jankowski R. (2017). Damage-Involved Structural Pounding in Bridges under Seismic Excitation, Key Eng. Mater., 754:309–312, doi.org/10.4028/www.scientific.net/KEM.754.309.

Jankowski R. (2005). Non-Linear Viscoelastic Modelling of Earthquake-Induced Structural Pounding, Earthq. Eng. Struct. Dyn., 34(6):595–611, doi.org/10.1002/eqe.434.

Jiao C., Lu J., Wang C., Long P., Sun Z. (2021). Experimental and Numerical Investigations on the Effects of Radius of Curvature and Longitudinal Slope on the Responses of Curved Bridges Subject to Seismic Pounding, Meas. Control, 54(3–4):519–37, doi.org/10.1177/00202940211000377.

Jónsson M.H., Bessason B., Haflidason E. (2010). Earthquake Response of a Base-Isolated Bridge Subjected to Strong near-Fault Ground Motion, Soil. Dyn. Earthq. Eng., 30 (6): 447–55, doi.org/10.1016/j.soildyn.2010.01.001.

Kasai, K., Maison B. F. (1997). Building Pounding Damage during the 1989 Loma Prieta Earthquake, Eng. Struct., 19 (3): 195–207, doi.org/10.1016/S0141-0296(96)00082-X.

Kaviani P., Zareian F. (2014). Performance-Based Seismic Assessment of Skewed Bridges, PEER Report No. 2014/01, Pacific Earthquake Engineering Research Center, University of California, Berkeley, CA.

Kaviani P., Zareian F., Taciroglu E. (2012). Seismic Behavior of Reinforced Concrete Bridges with Skew-Angled Seat-Type Abutments, Eng. Struct., 45:137–50, doi.org/10.1016/j.engstruct.2012.06.013.

Kawashima K. (2012). Damage of Bridges Due To the 2011 Great East Japan Earthquake, Journal of Japan Association for Earthquake Eng., 12 (4): 319–38. doi.org/10.5610/jaee.12.4_319.

Kawashima K., Shigeki U., Jun I. H., Kenji K. (2011). Damage of Bridges Due to the 2010 Maule, Chile, Earthquake, Journal of Earthquake Eng. 15 (7): 1036–68, doi.org/10.1080/13632469.2011.575531.

Kikuchi M., Nakamura T., Aiken I.D. (2010). Three-Dimensional Analysis for Square Seismic Isolation Bearings under Large Shear Deformations and High Axial Loads, Earthq. Eng. Struct. Dyn., 39(13):1513–31, doi.org/10.1002/eqe.1042.

Konstantinidis D., Kelly J.M., Makris N. (2008). Experimental Investigation on the Seismic Response of Bridge Bearings, Report EERC-2008/02, Earthquake Engineering Research Center, University of California, Berkeley, CA

Kumar M., Whittaker A.S., Constantinou M.C. (2015). Seismic Isolation of Nuclear Power Plants, Tech. Rep. MCEER-15-0008, MCEER, Buffalo, NY

Kikuch M., Aiken I.D. (1997). An Analytical Hysteresis Model for Elastomeric Seismic Isolation Bearings, Earthq. Eng. Struct. Dyn., 26(2):215–31, doi.org/10.1002/(SICI)1096-9845(199702)26:2<215::AID-EQE640>3.0.CO;2-9.

Kumar M., Whittaker A.S., Constantinou M.C. (2013). Mechanical Properties of Elastomeric Seismic Isolation Bearings for Analysis Under Extreme, Proceedings, 22nd International Conference on Structural Mechanics in Reactor Technology (SMiRT 22), San Francisco, CA

Kun C., Jiang L., Chouw N. (2017). Influence of Pounding and Skew Angle on Seismic Response of Bridges, Eng. Struct., 148:890–906, doi.org/10.1016/j.engstruct.2017.07.024.

Lankarani H.M., Nikravesh P. E. (1990). A Contact Force Model With Hysteresis Damping for Impact Analysis of Multibody Systems, J. Mech. Design, 112(3):369–76, doi.org/10.1115/1.2912617.

Lee Marsh M., Stringer S.J. (2013). *Performance-based seismic bridge design, a synthesis of highway practice,* Vol 440, Transportation Research Board, Washington, DC.

Li J., Peng T., Xu Y. (2008). Damage Investigation of Girder Bridges under the Wenchuan Earthquake and Corresponding Seismic Design Recommendations. Earthq. Eng. Eng. Vib., 7(4): 337–44, doi.org/10.1007/s11803-008-1005-6.

Malhotra P.K., Huang M.J., Shakal A.F. (1995). Seismic Interaction at Separation Joints of an Instrumented Concrete Bridge, Earthq. Eng. Struct. Dyn., 24(8):1055–67, doi.org/10.1002/eqe.4290240802.

Marquez J.F. (2021). Modeling of Lead Rubber Bearings at Large Strains and Effects on Structural Response, PhD thesis, University of California San Diego, San Diego, CA.

Masroor A., Mosqueda G. (2013). Impact model for simulation of base isolated buildings impacting flexible moat walls, Earthq. Eng. Struct. Dyn., 42:357-376, https://doi.org/10.1002/eqe.2210

McKenna F., Scott M.H., Fenves G.L. (2010). Nonlinear finite-element analysis software architecture using object composition, J. Comp. Civil Eng., 24(1):95-107, doi.org/10.1061/(ASCE)CP.1943-5487.0000002.

Mitchell D., Tinawi R., Sexsmith R. G. 1991. Performance of Bridges in the 1989 Loma Prieta Earthquake - Lessons for Canadian Designers, Can. J. Civil Eng., 18(4): 711–34, doi.org/10.1139/l91-085.

Muthukumar S., DesRoches R. (2006). A Hertz Contact Model with Non-Linear Damping for Pounding Simulation, Earthq. Eng. Struct. Dyn., 35(7):811–28, doi.org/10.1002/eqe.557.

Nakamura T. (2012). Behaviors of Lead Rubber Bearing under Horizontal Bi-Directional Loading Test, Proceedings, 15th World Conference on Earthquake Engineering, Lisbon, Portugal.

Nishi T., Suzuki S., Aoki M., Sawada T., Fukuda S. (2019). International Investigation of Shear Displacement Capacity of Various Elastomeric Seismic-Protection Isolators for Buildings, J. Rubber Research, 22 (1): 33–41, doi.org/10.1007/s42464-019-00006-x.

Padgett J.E., Nielson B.G., DesRoches R. (2008). Selection of Optimal Intensity Measures in Probabilistic Seismic Demand Models of Highway Bridge Portfolios, Earthq. Eng. Struct. Dyn., 37(5):711–25, doi.org/10.1002/eqe.782.

Paulay T., Priestly M. J. N. (1992). *Seismic Design of Reinforced Concrete and Masonry Buildings,* 1st ed., John Wiley & Sons

Priestley M. J. N., Seible F., Calvi G. M. (1996). *Seismic Design and Retrofit of Bridges*, 1st ed., John Wiley & Sons

Ramanathan K. (2012). Next Generation Seismic Fragility Curves for California Bridges Incorporating the Evolution in Seismic Design Philosophy, PhD thesis, Georgia Institute of Technology, Atlanta, GA.

Rezaei H., Moayyedi S.A., Jankowski R. (2020). Probabilistic Seismic Assessment of RC Box-Girder Highway Bridges with Unequal-Height Piers Subjected to Earthquake-Induced Pounding. Bull. Earthq. Eng., 18 1547–1578, doi.org/10.1007/s10518-019-00764-4.

Robinson W. H. (1998). Passive Control of Structures, the New Zealand Experience, ISET J. Earthq. Technol., 35(4):63–75.

Ruangrassamee A., Kawashima K. (2001). Relative displacement response spectra with pounding effect, Earthq. Eng. Struct. Dyn., 30:1511-1538, https://doi.org/10.1002/eqe.75

Ryan K.L., Polanco J. (2008). Problems with Rayleigh Damping in Base-Isolated Buildings, J. Struct. Eng., 134(11):1780–84, doi.org/10.1061/(asce)0733-9445(2008)134:11(1780).

Saatcioglu M., Razvi S.R. (1992). Strength and Ductility of Confined Concrete, J. Struct. Eng., 118(6):1590–1607, doi.org/10.1061/(asce)0733-9445(1992)118:6(1590).

Sanchez J., Masroor A., Mosqueda G., Ryan K. (2013). Static and Dynamic Stability of Elastomeric Bearings for Seismic Protection of Structures, J. Struct. Eng., 139(7):1149-1159, doi.org/10.1061/(ASCE)ST.1943-541X.0000660

Sarebanha A. (2018). Experimental and Numerical Simulation of Seismically Isolated Critical Facilities under Extreme Seismic Loading, PhD thesis, University of California San Diego, San Diego, CA.

Sarebanha A., Mosqueda G., Kim M.K., Kim J.H. (2018). Seismic response of base isolated nuclear power plants considering impact to moat walls, Nucl. Eng. Des., 328:58-72, 10.1016/j.nucengdes.2017.12.021.

Scott B.D. (1980). Stress-Strain Relationships for Confined Concrete: Rectangular Sections, PhD Thesis, The University of Canterbury, Canterbury, New Zealand.

Scott M.H., Fenves G.L. (2006). Plastic Hinge Integration Methods for Force-Based Beam–Column Elements, J. Struct. Eng., 132(2):244–52, doi.org/10.1061/(asce)0733-9445(2006)132:2(244).

Tsiavos A., Stojadinovic B., Mackie K. (2014). Dynamics of Inelastic Isolated Bridges Subjected to Analytical Pulse Ground Motions, Proceedings, 10th U.S. National Conference on Earthquake Engineering, Anchorage, AK.

Unanwa C., Mahan M. (2014). Statistical Analysis of Concrete Compressive Strengths for California Highway Bridges, J. Perf. Constr. Facil., 28(1):157–67, doi.org/10.1061/(asce)cf.1943-5509.0000404.

USGS (2022). U.S. geological survey unified hazard tool, https://earthquake.usgs.gov/hazards/interactive/

Vosooghi A., Saiidi M.S. (2010). Seismic Damage States and Response Parameters for Bridge Columns, ACI Spec. Publ., 271:29–46, doi: 10.14359/51663888

Wilson P., Elgamal A. (2010). Large-Scale Passive Earth Pressure Load-Displacement Tests and Numerical Simulation, J. Geotech. Geoenviron. Eng., 136(12):1634–43, doi.org/10.1061/(ASCE)GT.1943-5606.0000386.

Xiang N., Li J. (2018). Effect of Exterior Concrete Shear Keys on the Seismic Performance of Laminated Rubber Bearing-Supported Highway Bridges in China, Soil. Dyn. Earthq. Eng., 112(5): 185–97, doi.org/10.1016/j.soildyn.2018.04.033.

Yamamoto S., Kikuchi M., Ueda M., Aiken I.D. (2008). Analytical Modeling of Elastomeric Isolation Bearings Under Severe Axial Load and Shear Deformations, Proceedings, 14th World Conference on Earthquake Engineering, Beijing, China.

Zhang J., Huo Y. (2009). Evaluating Effectiveness and Optimum Design of Isolation Devices for Highway Bridges Using the Fragility Function Method, Eng. Struct., 31(8):1648–60, doi.org/10.1016/j.engstruct.2009.02.017.

The Pacific Earthquake Engineering Research Center (PEER) is a multi-institutional research and education center with headquarters at the University of California, Berkeley. Investigators from over 20 universities, several consulting companies, and researchers at various state and federal government agencies contribute to research programs focused on performance-based earthquake engineering.

These research programs aim to identify and reduce the risks from major earthquakes to life safety and to the economy by including research in a wide variety of disciplines including structural and geotechnical engineering, geology/seismology, lifelines, transportation, architecture, economics, risk management, and public policy.

PEER is supported by federal, state, local, and regional agencies, together with industry partners.

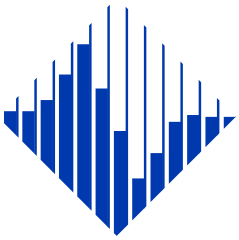

PEER Core Institutions

University of California, Berkeley (Lead Institution)
California Institute of Technology
Oregon State University
Stanford University
University of California, Davis
University of California, Irvine
University of California, Los Angeles
University of California, San Diego
University of Nevada, Reno
University of Southern California
University of Washington

Pacific Earthquake Engineering Research Center
University of California, Berkeley
325 Davis Hall, Mail Code 1792
Berkeley, CA 94720-1792
Tel: 510-642-3437
Email: peer_center@berkeley.edu

ISSN 2770-8314
https://doi.org/10.55461/YWIX6500